

**Fabrication of GCN (Graphitic Carbon
Nitride) Nanosheets Based CA
(Cellulose Acetate) Mixed Matrix
Membranes for Carbon Capture**



By

Mubashir Ahmed

School of Chemical and Materials Engineering

National University of Science and Technology

2023

**Fabrication of GCN (Graphitic Carbon
Nitride) Nanosheets Based CA
(Cellulose Acetate) Mixed Matrix
Membranes for Carbon Capture**



Name: Mubashir Ahmed

Registration Number: 00000319872

**This thesis is submitted as a partial fulfillment of the requirements
for the degree of**

MS Chemical Engineering

Supervisor Name: Dr. Sarah Farrukh

School of Chemical and Materials Engineering (SCME)

National University of Science and Technology (NUST)

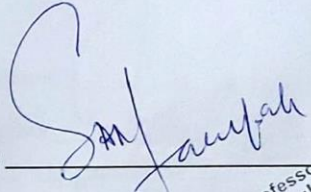
H-12 Islamabad, Pakistan

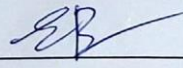
May, 2023

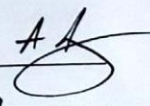


THESIS ACCEPTANCE CERTIFICATE

Certified that final copy of MS thesis written by Mr **Mubashir Ahmed** (Regn No 00000319872), of School of Chemical & Materials Engineering (SCME) has been vetted by undersigned, found complete in all respects as per NUST Statues/Regulations, is free of plagiarism, errors, and mistakes and is accepted as partial fulfillment for award of MS degree. It is further certified that necessary amendments as pointed out by GEC members of the scholar have also been incorporated in the said thesis.

Signature: 
Name of Supervisor: **Dr Sarah Farrukh**
Date: 12/7/2021
Associate Professor
Dr Sarah Farrukh
School of Chemical and Materials
Engineering (SCME-NUST)
ISLAMABAD

Signature (HOD): 
Date: 4/8/23

Signature (Dean/Principal): 
Date: 4-8-2023



National University of Sciences & Technology
(NUST)

MASTER'S THESIS WORK

Formulation of Guidance and Examination Committee (GEC)

Name: Mubashir Ahmed
Department: SCME
Credit Hour Completed: 18 / 24

NUST Regn No: 00000319872
Specialization: MS Chemical Engineering
CGPA: 3.25

Course Work Completed

S/No	Code	Title	Core/Elective	CH	Grade
1	CHE 843	Separation processes in Chemical Engineering	Core	3	B+
2	EME 921	Momentum Heat and Mass transfer Chemical Engineering	Core	3	C+
3	ENE 809	Wastewater Treatment and Design	Elective	3	B+
4	RM 898	Research Methodology	Additional	2	Q
5	CHE 847	Chemical Kinetics and Reactor Design	Core	3	B
6	CHE 873	Membrane Technology	Elective	3	B+
7	ESE 911	Carbon Capture and Utilization	Elective	3	B+
8	CHE 848	<u>Gasification Processes</u> <u>Nano catalysis</u>	Elective	3	B

Date: 15/2/2021

Student's Signature: Mubashir

Exam Branch
23/2/21

Thesis Committee

- Name: Dr. Sarah Farukh (Supervisor)
Department: Chemical Engineering (SCME)
- Name: Dr. Zaib Jahan (Co-Supervisor)
Department: Chemical Engineering (SCME)
- Name: Dr. Tayyaba Noor
Department: Chemical Engineering (SCME)
- Name: Lecturer Ayesha Raza
Department: Chemical Engineering (SCME)
- Name: _____
Department: _____

Signature: Sarah Farukh

Signature: Zaib Jahan

Signature: Tayyaba Noor

Signature: Ayesha Raza

Date: 19/2/2021

Signature of Head of Department: Mubashir

APPROVAL

Dean/Principal Af

Date: 22/2/2021

Distribution

- 1x copy to Exam Branch, Main Office NUST
- 1x copy to PGP Dte, Main Office NUST
- 1x copy to Exam branch, respective institute

School of Chemical and Materials Engineering (SCME) Sector H-12, Islamabad



Form: TH-04

National University of Sciences & Technology (NUST)

MASTER'S THESIS WORK

We hereby recommend that the dissertation prepared under our supervision by

Regn No & Name: 00000319872 Mubashir Ahmed

Title: Fabrication of GCN (Graphitic Carbon Nitride) Nanosheets based CA (Cellulose Acetate) Mixed Matrix Membranes for Carbon Capture.

Presented on: 15 Jun 2023 at: 1400 hrs in SCME Seminar Hall

Be accepted in partial fulfillment of the requirements for the award of Master of Science degree in Chemical Engineering.

Guidance & Examination Committee Members

Name: Dr Ayesha Raza

Signature: [Signature]

Name: Dr Tayyaba Noor

Signature: [Signature]

Name: Dr Zaib Jahan (Co-Supervisor)

Signature: [Signature]

Supervisor's Name: Dr Sarah Farrukh

Signature: [Signature]

Dated: 15/6/2023

Head of Department

Date: 3/7/23

Dean/Principal

Date: 3-7-2023

School of Chemical & Materials Engineering (SCME)

Dedication

I dedicate this work to my beloved parents, friends, respectable teachers and especially thanks to my supervisor, whose continuous and tireless support makes this work possible.

Acknowledgements

All praise is due to **Almighty Allah**, the Most Benevolent, the Most Compassionate, Who has provided me with the fortitude, self-assurance, and strength to complete my research and overcome all obstacles in my path. It is a great blessing that I was able to complete this task within the allotted time frame.

My supervisor, **Dr. Sarah Farrukh**, has been an invaluable resource during my master's thesis research. She has always believed in me and supported me, for which I am profoundly grateful. I would also like to thank my co-supervisor, **Dr. Zeb Jahan**, who provided me with excellent research guidance throughout the duration of this assignment.

I would also like to appreciate the members of my Guidance and Examination Committee (GEC), **Dr. Tayyaba Noor** and **Dr. Ayesha Raza**, for their assistance in resolving the issues with my research project. I am also appreciative of their moral support and material assistance.

I would also want to express my appreciation to the Lab's personnel for their help with the required characterization tests. I am thankful, especially to Mr. Zarrar Salah ud din from MEMAR Lab, Mr. Zafar from SEM Lab, Mr. Nouman from Chemical analysis Lab, Mr. Hamza from XRD Lab and Mr. Khawar from Mechanical Testing Lab SCME NUST.

Lastly, I would like to express my appreciation to my family and friends, who have always supported and encouraged me, particularly when I've encountered difficulties with my work. They provided me with the emotional support and assistance I required to complete my research.

Abstract

In recent years, there has been an increasing demand for efficient separation technologies for CO₂/CH₄ gas mixtures, particularly in the natural gas processing industry. The separation of CO₂ from CH₄ is crucial to produce natural gas with a high heating value and reduced greenhouse gas emissions. Due to their low energy requirements, scalability, and affordability, membrane-based gas separation technologies have become a possible replacement for conventional separation techniques. In gas separation applications, mixed matrix membranes (MMMs), which incorporate the benefits of both polymers and inorganic materials, have gained a lot of interest. In this study, 2D graphitic carbon nitride nanosheets (g-C₃N₄) were added to the polymer matrix to enhance the performance of cellulose acetate MMMs for CO₂/CH₄ gas separation. The solution casting process was used to create CA based MMMs with different g-C₃N₄ loadings like 0.5, 1.0 and 1.5 wt% using tetrahydrofuran (THF) as solvent. FTIR, XRD, SEM, UTM and permeation studies were used to characterize the produced MMMs. Incorporation of GCN into CA polymer matrix enhances its Thermal and Mechanical stability. It was found that GCN based CA MMMs give better CO₂/CH₄ selectivity of 2.73 at a GCN loading of 0.5 wt% with CO₂ permeability of 78 Barrer at 2 bars. A more compact and dense structure could be seen in the SEM images, FTIR confirms the presence of functional groups, XRD confirms the presence of GCN nanosheets in the MMMs. Moreover, maximum tensile strength of 81.66 MPa was shown by 0.5 wt% g-C₃N₄/CA mixed matrix membrane. In this study, results suggest that addition of GCN into CA polymer matrix enhances CO₂ gas permeability having less impact on CO₂/CH₄ selectivity, further research should be carried out to improve selectivity of these membranes.

Table of Contents

Dedication	i
Acknowledgements	ii
Abstract	iii
Table of Contents	iv
List of Figures	vi
List of Tables	vii
Nomenclature	viii
Chapter 1	1
Introduction	1
1.1 Background.....	1
1.2 Membrane separation:.....	5
1.3 Polymeric membrane:	6
1.4 Polymer Blend Membranes:	7
1.5 Mixed Matrix Membranes:	8
1.6 Graphitic carbon nitride:	8
1.7 Cellulose Acetate:	10
1.8 Motivation:.....	11
Outline of the Thesis.....	12
Chapter 2	13
Literature Review.....	13
2.1 CA based mixed matrix membranes (MMMs):	13
2.2 Graphitic carbon nitride (g-C ₃ N ₄) based mix matrix membranes:	16
Chapter 3	18
Experimental Methods	18
3.1 Materials used:	18
3.2 Synthesis of pure CA membrane:	18
3.3 Fabrication of Mixed Matrix Membranes:.....	18
3.4 Testing and Characterization	19
3.4.1 Scanning Electron Microscopy (SEM)	19
3.4.1.1 Components of SEM.....	19
3.4.1.2 SEM Working Principles	20
3.4.2 Fourier transform Infrared (FT-IR) Spectroscopy	20
3.4.2.1 Components of FT-IR Spectrometer.....	21
3.4.2.2 Working Principles	22
3.4.3 X-Ray Diffraction (XRD)	22

3.4.4 Gas Permeation Testing	24
3.4.5 Mechanical Testing.....	26
Chapter 4.....	28
Results and Discussion	28
4.1 Characterization techniques:.....	28
4.1.1 Fourier Transform Infra-Red (FT-IR) Spectroscopy:	28
4.1.2 Mechanical Testing:.....	31
4.1.3 Scanning Electron microscopy (SEM) analysis:.....	32
4.1.4 XRD Analysis:	34
4.1.5 Gas Permeation Testing:	36
Conclusion	41
References.....	42

List of Figures

Figure 1.1. Worldwide fossil CO ₂ emissions.....	1
Figure 1.2. g-C ₃ N ₄ nanosheets structure	9
Figure 1.3 Cellulose acetate structure	10
Figure 3. 1 Schematic diagram of scanning electron microscopy (SEM) machine [48, 49]	20
Figure 3. 2 Schematic diagram of Fourier Transform Infrared (FT-IR) Spectrometer	21
Figure 3. 3 Different modes of molecular vibration in FT-IR (stretching and bending)	22
Figure 3. 4 Schematic diagram of X-Ray Diffraction characterization	23
Figure 3. 5 Bragg's Law X-Ray Diffraction system.....	24
Figure 3. 6 Gas permeation testing system rig.....	25
Figure 3. 7 stress-strain behavior of several classes of materials	27
Figure 3. 8 Schematic diagram of ultimate tensile testing system.....	27
Figure 4. 1 Pure CA membrane's FTIR spectrum.....	29
Figure 4. 2 FTIR spectrum of CA/g-C ₃ N ₄ MMMs	30
Figure 4. 3 Ultimate tensile strength for membrane samples with g-C ₃ N ₄ loading of 0%, 0.5%, 1.0%, and 1.5%.....	32
Figure 4. 4 SEM images of membrane samples (i)Pure CA surface (ii) Pure CA cross-section (iii)surface of g-C ₃ N ₄ /CA 0.5 wt% (iv) Cross surface of g-C ₃ N ₄ /CA 0.5 wt%	33
Figure 4. 5 SEM images of membrane samples (v) surface of g-C ₃ N ₄ /CA 1 wt% (vi) cross-section of g-C ₃ N ₄ /CA 1 wt% (vii) surface of g-C ₃ N ₄ /CA 1.5 wt% (viii) cross-section of g-C ₃ N ₄ /CA 1.5 wt%	34
Figure 4. 6 XRD pattern of (i) pure CA and (ii) g-C ₃ N ₄ nanosheets	35
Figure 4. 7 XRD pattern of g-C ₃ N ₄ /CA MMMs with different wt.%	36
.....	38
Figure 4.8 b Permeability of CO ₂ with pressure	38
Figure 4.8 a Permeability of CH ₄ with pressure	38
Figure 4.8 a CO ₂ /CH ₄ selectivity of MMM's	40

List of Tables

Table 1. 1 Typical composition of Natural gas	2
Table 1. 2 Relationship between the number of people (in thousands) and the amount of energy used (in thousands of metric tonnes of oil equivalent)[5]	3
Table 2. 1 Literature review of g-C ₃ N ₄ nanosheets mixed matrix membranes.....	17
Table 4.1 Gas permeation testing:.....	37

Nomenclature

CA	Cellulose acetate
GCN	graphitic Carbon Nitride
GPU	Gas permeation unit
MOF	Metal Organic Framework
CNT	Carbon nanotubes
SEM	Scanning Electron Microscopy
XRD	X-ray Diffraction
MWCNT	multiwall carbon nanotubes
SBR	styrene butadiene rubber
FTIR	Fourier transform Infrared Spectroscopy
THF	Tetrahydrofuran
GO	Graphene Oxide

Chapter 1

Introduction

1.1 Background

Energy resources are in ever-increasing demand as the world's population rises daily. Industrial production of commodities has increased as well to keep up with the demands of the expanding population. The increased industrial output necessitates energy. Fossil fuels have been able to provide this demand since the 18th century.

As for as Global Emission of carbon dioxide is concerned, nearly 412 parts per million (ppm) of carbon dioxide are present in the Earth's atmosphere, and that number is increasing. Since 2000, when it reached 370 ppm, it has increased by 11%, and since the beginning of the Industrial Age, when it was close to 280 ppm, it has increased by 47%.

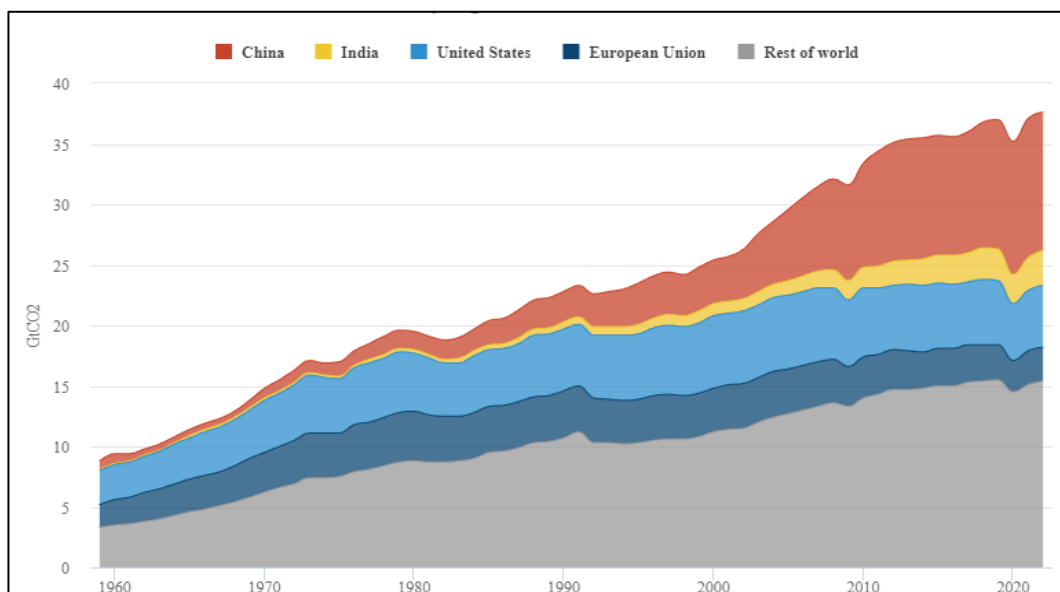


Figure 1.1. Worldwide fossil CO₂ emissions

Despite an uncertainty range of 0.1% to 1.9% in 2022 and a relatively modest increase of 1.0%, it is expected that worldwide fossil CO₂ emissions will surpass the pre-pandemic peak in 2019 and break a new record with 36.6 billion tonnes of CO₂.as shown in figure 1.1 .[1]

Energy for both industrial and domestic use is primarily derived from natural gas. Methane is the primary combustible component of natural gas, with traces of ethane and propane. In addition to the principal components, natural gas also contains a significant number of impurities, such as carbon monoxide (CO), carbon dioxide (CO₂), hydrogen sulfide (H₂S), and sulfur dioxide (SO₂)[2]. When compared to pure natural gas. **Table 1.1** lists the typical composition of natural gas. Wasiu et al. observed that an increase in carbon dioxide lowers the heating value of natural gas. This has been demonstrated in many tests, where a variety of natural gas mixtures with various CO₂ contents were used. It was observed that the flame velocity, rate of combustion, and heat produced by the reaction all reduced as the amount of CO₂ rose[3].

Table 1. 1 Typical composition of Natural gas

Name	Volume %
Methane	>85
Ethane	3-8
Propane	1-2
Butane	<1
Pentane	<1
Carbon Dioxide	1-2
Hydrogen Sulfide	<1
Nitrogen	1-5
Helium	<0.5

Additionally, the demand for energy worldwide rises along with the world population. Between 1990 and 2020, the global population is predicted to grow by a factor of 1.1%, whilst the energy consumption is predicted to grow by 2.2% [4]. Another estimate from the year 2000 for 14 European nations looked at the relationship between energy use and population at the time. The results showed a pattern that suggested that as the population grew, so did energy use, as seen in Table 1.2 [5].

Table 1. 2 Relationship between the number of people (in thousands) and the amount of energy used (in thousands of metric tonnes of oil equivalent) [5]

Year	Population	Energy Consumption
2000	376,037	1,460,284
2025-Lower	374,902	1,805,297
2025-Medium	393,659	1,953,477
2025-Higher	412,144	2,101,007

As a result, growing populations call for greater energy output, which in turn calls for more fuel supplies. We already have a very rapid depletion of our fuel resources. According to research done by N.A. Owen et al., oil reserves increased in the early 1900s, particularly from 1930 onwards. However, after 1972, the oil supplies began to run out. This indicates that more oil was extracted from the reservoirs than was discovered there. After 1980, the reserves were steadily running out, which showed that the supply of traditional energy sources was declining [6]. As we've already seen, adding CO₂ lowers the energy output of fuel gases. Therefore, if we want to enhance the output from conventional energy sources, we must lower the CO₂ content of the natural gas being used. When distributing natural gas, it is required that CO₂ levels be kept at or below 2%. [7]

Therefore, it is necessary to remove CO₂ from different gas streams, such as the sweetening of natural gas and the purification of biogas. [8]

As a result, the CO₂ that is extracted from these sources is in a highly concentrated state that may be used for enhanced oil recovery in oil and gas wells as well as being stored in vast subterranean reserves through the carbon sequestration process.

We have a number of approaches, including gas adsorption on solid surfaces, membrane gas separation, and gas absorption through liquids, for the aim of separating CO₂ from different gases, including natural gas[9, 10]. The two approaches that have been most extensively studied and are thought to be the most effective for separating CO₂ are liquid gas absorption and adsorption on solid surfaces. Both of these methods for gas separation are widely employed in the business. These two approaches do have some disadvantages, with the primary one being that they both require a lot of energy. This indicates that the additional energy required to remove or capture the carbon dioxide gas balances out the energy saved by reducing the carbon dioxide content of natural gas.[11]

Research has been going on to identify a technique or process that is less energy-intensive and more energy-efficient for CO₂ separation. The most effective method that satisfies these requirements, according to decades of research, is membrane gas separation since it consumes a lot less energy than traditional gas separation methods. About 40–50% of the energy required by these thermally demanding procedures is consumed by membrane processes[12]. Due to their ease of manufacture, integration into current industries, and scale-up, membranes are also a very promising technique to replace the traditional separation methods. Materials such as ceramics, metals, glass, and polymers are used to make membranes.[13, 14]

We chose polymers as our preferred medium for membrane production because of the economic benefit they provide and the simplicity with which a membrane may be made utilising polymers[15]. Additionally, we used glassy polymers out of all the available polymers due to the effective gas separation they provide due to their stiff and fixed pores.[16]

1.2 Membrane separation:

Membrane separation has received a lot of attention from both academic institutions and several corporate sectors since it offers the most dependable and efficient way to address environmental problems. The physical and chemical characteristics of the material used to fabricate gas separation membranes should be such that they can successfully separate one component from a mixture. For a membrane material to work for a longer amount of time, it must also have sufficient mechanical and chemical stability. The following variables affect the membrane's ability to separate gases.

- Membrane conversion into a module for use on a commercial scale (e.g. flat sheet, spiral wound, hollow fibre etc.)
- Membrane module.
- Membrane structure.
- Material.[12]

Permeability and selectivity of a membrane are key factors for enhanced gas separation performance. The rate at which elements can pass through a membrane is known as permeability. It depends upon Kinetic factor and Thermodynamic factor. The next fundamental factor is selectivity, which refers to a membrane's natural ability to let one component through a mixture more readily than another. Additionally, it's a crucial factor in obtaining greater product purity at high recoveries. Gas separation membrane will develop significantly if more selective membranes are manufactured[17].

One of the most important steps in separation procedures is the choice of materials for the manufacturing of the membrane. For the manufacture of membranes, specific material choices are selected based on the desired chemical properties of the material. Based on how the component interacts with the membrane material, a component can be effectively separated from a mixture. The separation efficiency of the membrane is improved if the membrane material has certain functional groups that generate an affinity for a particular gas from the mixture. As a result, one gas separates more easily than the others. Membranes are made from materials such as ceramics, glass, metals, and polymers.[18, 19].

1.3 Polymeric membrane:

Ceramics, glass, metals, and polymers are among the many materials that may be used to create membranes. Out of all of these materials, we chose polymers as our preferred medium for membrane manufacturing due to the cost benefit they provide and the simplicity with which a membrane may be made utilising polymers. In general, polymers showed higher selectivities and lower throughput when compared to porous material since there was less free volume available. Polymers are more effective at transferring one chemical species from a mixture of gases to another. Gases pass across porous and dense gas separation membranes, respectively, according to the Knudsen diffusion and solution diffusion models. Increased permeability will cause less selectivity in polymeric membranes, and vice versa. In addition, Robeson established upper bound limits for permeability/selectivity in a graph by displaying the values of permeability obtained of tiny gaseous molecules, primarily CO₂, N₂, CH₄, and O₂, which permeate through polymeric membranes made of various polymers. For gas separation, polymeric membranes that are dense or impermeable are typically used. Within a polymer, gases are separated based on their individual diffusion and solubility coefficients.[20, 21]

Because glassy polymers offer higher selectivity and lower permeability for various gas combinations, including CO₂/CH₄, O₂/N₂, and H₂/CH₄, they are more acceptable for use in the manufacture of dense polymeric membranes than rubbery polymers.

Single polymer membranes were initially employed for this purpose when membrane gas separation was a new technique. M.W. Tang et al. examined various solvent-made cellulose acetate membranes for CO₂/CH₄ separation in a specific research study. Heptane, octane, nonane, decane, toluene, and xylene were only a few of the solvents used to make these cellulose acetate membranes. The membranes had a maximum CO₂ permeance of 216 GPU (Gas Permeation Unit), while their CO₂/CH₄ selectivity was 36.[22]

Later, as research grew, it was observed that polymeric materials reduce the effectiveness of separation of gases using current membrane technology. Therefore, innovative resources are required to improve the efficiency of gas separation. Membranes made of a polymer blend were therefore recommended for enhancing gas separation efficiency. The best feature of blend membranes is how they mix two

polymers' positive traits into a single membrane. For instance, combining a tough polymer with one that is highly permeable can provide both high permeability and mechanical toughness. Combining a highly porous polymer with a highly selective polymer is another way to create a blend. If a solution system is required for the solubility of the polymers, they might either be immiscible or miscible when dissolved in a common solvent. A mixture of miscible polymers has a homogenous composition, appears as a single phase, and exhibits a single value for both the melting point and the glass transition point.[23, 24]

Ceramics, metals, and carbon that has been thermally decomposed can also be used to create membranes. These membranes include zeolites and carbon molecular sieves, which have significantly higher selectivity and permeability compared to polymeric materials. However, due to their inherent brittleness, these materials make it extremely difficult to create continuous-phase membranes that are devoid of cracks and other discontinuities. Additionally, they are highly expensive to produce, which poses significant obstacles to their application as an independent membrane material[15].

In contrast to either fully polymeric or completely inorganic membranes, mixed matrix membranes that have a discrete inorganic phase and a continuous polymer phase are hence preferable for use in gas separation[12]. Additionally, since mixed matrix membranes are only a fundamental modification of the pure polymeric membrane, they are significantly simpler and more affordable to make. To enhance the effectiveness of membranes for gas separation, several filler particles have been used, including zeolites, carbon molecular sieves, and silica nanotubes. However, several novel materials are also being tested, such as metal organic frameworks and carbon nanotubes.[25]

1.4 Polymer Blend Membranes:

Miscible and immiscible blends of polymers are the two types that can exist. Every component of the membrane is dissolved in a single solvent when it is a miscible blend[23]. Blends of miscible polymers only have one phase since they are entirely dissolved in one another. Additionally, their composition alone determines how they behave. Glass transition temperature and melting temperature, for example, will have a single value as in a homo-polymer but will be composition-dependent[26].

In order to create an immiscible mixture, several polymers are dissolved in a solvent system. This is due to the fact that such polymers are not soluble in a single solvent. But in immiscible blends, the composition as well as the phase distribution will determine the characteristics, and the various phases will function as independent pure polymers.

In order to combine the benefits of two different polymers, we can utilize polymer blends. Immiscible polymer blends have the benefit of allowing us better control over membrane morphology than the other two types of blends. So, we can experiment with the blend's composition to see how it affects the final membrane's morphology [27].

1.5 Mixed Matrix Membranes:

The commercial scale requirement for chemical species separation is beyond the capacity of the available polymeric membrane materials. Selectivity suddenly decreases when an increase in permeability is attained, and vice versa. By adding inorganic filler particles to polymers to create a polymer/inorganic particle hybrid known as mixed matrix membrane [28].

Because these inorganic particles serve as molecular sieve to improve diffusivity and selectivity, polymer/inorganic particle hybrid membranes outperform pure polymer and polymer blend membranes in terms of separation performance. The most often employed inorganic particles are metal organic frameworks (MOFs), zeolites, and carbon nanotubes (CNTs) [29, 30].

1.6 Graphitic carbon nitride:

Researchers have been interested in graphitic carbon nitride (g- C_3N_4) nanosheets because they can be used to modify membranes. The synthesis of g- C_3N_4 has a comparably long history, even though its use in membrane technology has only lately and steadily been researched. C_3N_4 polymer, often known as melon polymer, is one of the oldest synthetic polymers. Berzelius and Liebig initially reported on its production in 1834. As of now, g- C_3N_4 has been utilised in modifying membranes for a variety of applications, including water purification, gas separation, and ion exchange. In comparison to inorganic nanofillers like zeolites and particularly inorganic nanosheets

like NLDH, WS₂, etc., g-C₃N₄'s organic structure causes it to be more dispersible in a polymer matrix. [31]

As a result of the creation of NH₂ functional groups throughout g-C₃N₄ synthesis, no further functionalization is required for membrane formation and makes it hydrophilic in nature. g-C₃N₄ nanosheet is a two-dimensional semiconductor polymer composed of nitrogen and carbon atoms. g-C₃N₄ can be produced in a variety of allotropes depending on the materials used and the production process. g-C₃N₄ based on tri-s-triazine, which is the most energetically stable allotrope. Figure 1.2 shows that tri-s-triazine g-C₃N₄ nanosheets are made up of tri-s-triazine subunits (C₆ N₇) known as melem, are bonded through nitrogen atoms. It also shows that triangular nanopores are present having diameter of 3.11 Å, it is therefore clear that the presence of these triangular nanopores gives the g-C₃N₄ a molecular sieving ability that makes it suited for separation procedures.[32]

g-C₃N₄ nanosheets are fabricated from oxygen free, abundant and nitrogen free materials such as urea, cyanamide, thiourea, cyanuric chloride and melamine. In comparison to other semiconductors, the prevalence of g-C₃N₄ precursors is thought to be advantageous.

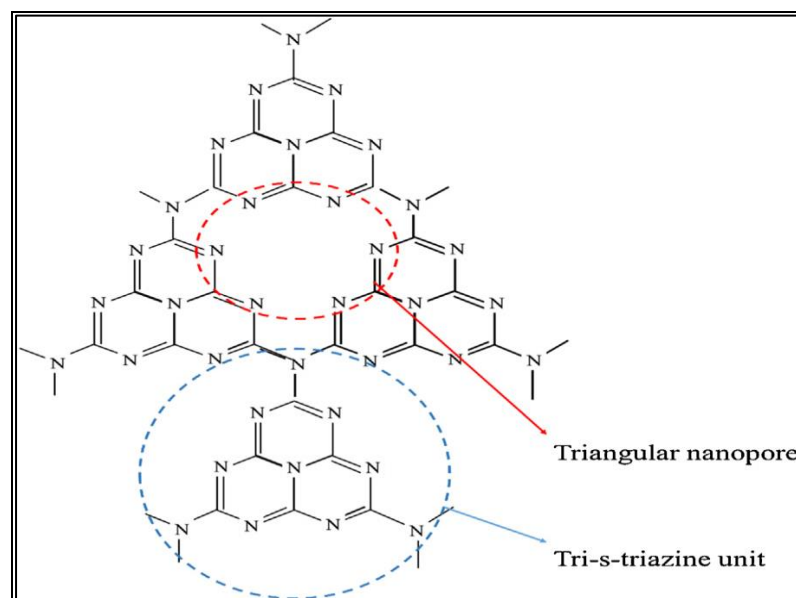


Figure 1.2. g-C₃N₄ nanosheets structure

1.7 Cellulose Acetate:

Cellulose acetate is the most popular polymer for the manufacture of membranes. According to history, cellulose acetate is a simple polymer that can be used to create membranes that remove CO₂ from natural gas. Often commercial scale membranes are fabricated from cellulose acetate. The hydroxyl (-OH) and carbonyl (C=O) groups in the main chain of CA-based membranes, which are used to separate CO₂ and CH₄ more effectively, increase the affinity of the membrane for CO₂ [33, 34]. Structure of CA is shown in figure 1.3. For fabrication of mixed matrix membrane, we have selected cellulose acetate and used graphitic carbon nitride (g-C₃N₄) nanosheets as filler. These membranes are put through permeation testing after manufacture for both pure CO₂ and pure CH₄ gas mixtures.

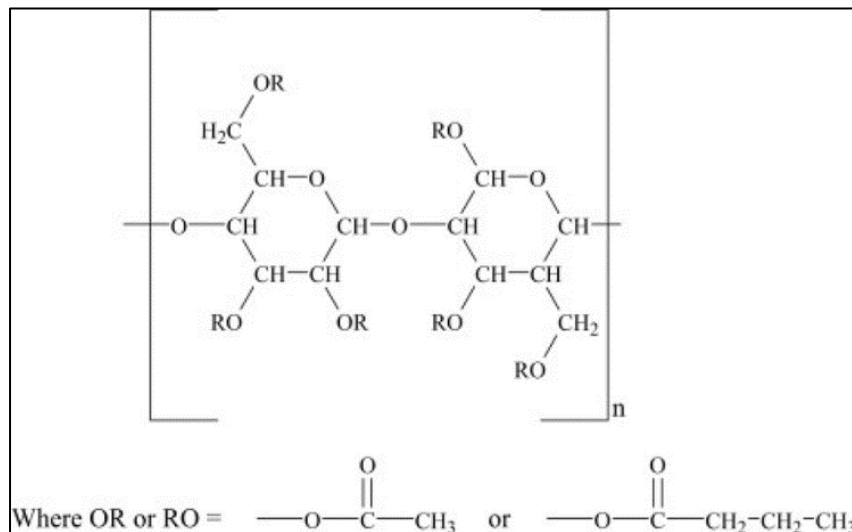


Figure 1.3 Cellulose acetate structure

1.8 Motivation:

We are interested in learning more about how g-C₃N₄ nanosheets affect the penetration of CO₂ via mixed matrix membranes. Additionally, we are interested in the impact of altering the filler particles in mixed matrix membranes on the membrane's ability to selectively allow CO₂ to permeate over CH₄. This research aims to increase the CO₂/CH₄ selectivity by using graphitic carbon nitride nanosheets in a mixed matrix membrane. This is done to make better use of the already available resources in order to tackle the ongoing energy crisis. Additionally, it lessens the strain on resources and restricts the negative effects of human activity on the environment. The objective of my research is:

- To fabricate 2D graphitic carbon nitride nanosheet based mixed matrix membranes.
- To investigate the result of incorporating g-C₃N₄ nanosheets to form a mixed matrix membrane and its advantage polymeric membranes.
- Characterization of the resulting membranes using the following techniques
 - Fourier Transform Infra-red (FT-IR) Spectroscopy
 - XRD analysis.
 - Scanning Electron Microscopy (SEM)
 - Tensile Strength Testing
- Finally, we want to evaluate how effectively the mixed matrix membranes separate, and recommend future advancements based on the results of that comparison.

Outline of the Thesis

1st Chapter details the introduction of polymer blends, their properties and their use in the separation of gas. This chapter also introduces 2D graphitic carbon nitride nanosheet and their uses in making mixed matrix membranes for gas separation.

2nd Chapter includes examples of the research work carried out in the use of g-C₃N₄ nanosheets in mixed matrix membranes for gas separation.

3rd Chapter summarizes the experimental techniques used to synthesize the mixed matrix and polymer blend membranes, and also the characterization techniques used to study their various physical and chemical properties.

4th Chapter studies the results obtained from different characterization techniques for all the fabricated membranes, and these results are then discussed in detail to explain their significance in my work.

5th Chapter gives a concise summary of the entire work and also lists recommendations for future work.

Chapter 2

Literature Review

As atmospheric carbon dioxide concentration rises, greenhouse gases that contribute to global warming will also grow. Around the world, efforts are being undertaken to lower the amount of CO₂ in the atmosphere using a variety of techniques, such as carbon dioxide sequestration and membrane systems to separate CO₂ from natural gas. Membrane separation is the most effective procedure. Membranes are used to separate it, and mixed matrix membrane systems are among the most popular study subjects and receive great praise.

2.1 CA based mixed matrix membranes (MMMs):

For the separation of CO₂/N₂, Hamidreza et al. determined the permeability through cellulose acetate/non-porous zeolite mixed matrix membrane. Cellulose acetate was used to create the membrane since it is the most popular and traditional polymer membrane material for separating CO₂ from N₂ and CH₄. Additionally, a large spiral-wound membrane module was produced on a commercial scale employing CA as the base matrix. Another product made from cellulose acetate was a hollow fibre membrane module used on offshore facilities to separate CO₂ from natural gas. In addition, CA has unusual properties that caused it to develop an affinity for the filler used to create the CA/filler mixed matrix membrane. In this study, NaY zeolite was added to the CA matrix, and the final mixture was poured onto a clear glass plate, with a doctor blade used to control the thickness. However, after further boosting the filler concentration (up to 25 wt%), a decrease in CO₂ permeability was seen. This was caused by the NaY zeolite concentration being increased from 0 to 20 wt%. With the loading of 0 to 15 wt%, the maximum increase in permeability for CO₂ is 4.9 barrers, and the drop in CO₂/N₂ selectivity from 26 to 18. Selectivity reached its peak at 20 weight percent filler loading before abruptly declining because of the percolation of particles in the membrane matrix. The aggregation of a higher concentration of filler is the cause of the reduced rise in diffusivity selectivity and greater drop in solubility selectivity in CA/NaY zeolite MMM. The permeability of CO₂ is also affected by changes in pressure, as a rise in pressure reduced the permeability of glassy polymers. Dual sorption model can be used to explain this decline in permeability[35].

The permeability and selectivity of CO₂ and CH₄ were determined by multiwall carbon nanotubes integrating into cellulose acetate matrix and manufacturing hybrid membrane. The incorporation of polyethylene glycol and cellulose acetate into carbon nanotubes (CNTs) has been investigated in acetone and the matrix of this work includes both. MWCNT helps with thermal stability, mechanical stability, and the long, convoluted pathway for carbon dioxide penetration, while PEG increases chain flexibility. The two portions of the permeation behaviour of gases are the first, which examines the effects of PEG and PEG/MWCNT weight percentages on single and mixed gas permeability as well as CO₂/CH₄ selectivity, and the second, which examines the effects of pressure on CO₂/CH₄ permeability and selectivity. Comparing CA/PEG blend membrane to neat CA, the latter has greater CO₂ and CH₄ permeability. Because cellulose acetate had neutral gaps between the polymeric chains, the irregular chain arrangement caused the formation of free volume, which is what caused an increase in CO₂ and CH₄ permeability and a decrease in CO₂/CH₄ selectivity. With the weight percentage of PEG remaining constant at 10%, MWCNT was added to CA in increments of 5 to 15%, and the permeability and selectivity of CO₂/CH₄ were observed. 10% PEG/CA was found to increase CO₂/CH₄ selectivity from 2.15 to 28.66, while the addition of 10% MWCNT increased CO₂/CH₄ selectivity from 28.66 to 38.4. Similar to this, when pressure increased, permeability dropped since there was less flow of gases due to the bigger pressure differential than there had been at lower pressures. The greatest findings for single and mixed gas selectivity of CO₂/CH₄ up to 48 and 38, respectively, are provided by 10% MWCNT/ 10% PEG/CA [36].

To investigate the penetration characteristics of both CO₂ and CH₄, cellulose acetate and titanium nanoparticle (TiO₂) were combined. Titania was chosen in part because it is a unique sort of semiconductor that, when combined with polymer, provides anti-fouling, thermal stability, and mechanical qualities to membrane. Additionally, TiO₂ can be used to analyse the gas permeation characteristics of H₂/N₂, O₂/N₂, H₂/CO₂, and CO₂/N₂ when introduced to polymer matrix. In this study, the penetrating characteristics of CO₂ and CH₄ gases were investigated while CA/TiO₂ MMM was synthesised using diffusion-induced phase separation techniques. TiO₂ integrated in the CA matrix with five different weight percentages, and 20% TiO₂ produced the greatest selectivity for CO₂/CH₄ [37].

By using the solution casting approach, A.R. Moghadassi et al. created cellulose acetate MMM blends with MWCNT, CA/PEG/MWCNT, and CA/styrene butadiene rubber (SBR)/MWCNT. The permeability and selectivity of CO₂/CH₄ were investigated using these membranes. The MWCNT utilised as filler was further divided into two categories: raw-MWCNT (R-MWCNT) and functionalized carboxylic acid-MWCNT (C MWCNT). Combining CA with SBR and adding MWCNT as filler improves the membranes' ability to withstand stress while also improving gas permeation performance. At 2 bar pressure, CA/MWCNT MMMs were investigated for permeability of helium, nitrogen, methane, and carbon dioxide as well as selectivity of CO₂/CH₄, CO₂/N₂, and N₂/CH₄. In general, permeability increases with increasing MWCNT loadings of all gases, and selectivity of CO₂/CH₄ and CO₂/N₂ increases, but selectivity for N₂/CH₄ decreases. In the case of CA/PEG/MWCNT, an increase in permeability was seen at CA/PEG/MWCNT-1% sample for all gases, and the highest selectivity was found at CA/PEG/MWCNT-0.5% sample for CO₂/CH₄, CO₂/N₂, and N₂/CH₄. In the final sample of CA/SBR/MWCNTs, the highest selectivity was found at CA/SBR/MWCNT-2% for CO₂/CH₄ and CO₂/N₂, and CA/SBR/MWCNT-1% for N₂/CH₄ [38].

The permeability and selectivity of CO₂, N₂, and CH₄ from NH₂-MIL-53(Al)/CA MMM were measured by Muhammad Mubashir et al. According to published research, adding amine functionalized metal-organic framework to polymeric matrix increased carbon dioxide permeability when compared to pure MOF-based MMM. An amine functionalized MOF with MIL-53 architecture is called NH₂-MIL-53(Al). Al³⁺ combined with the amine group to form a diamond shape with a 7.4Å aperture. Considerable resilience to high temperatures, optimised pore volume, and big surface area are some appealing qualities to utilise as filler for gas permeation studies. Furthermore, the presence of terephthalate ligands in NH₂-MIL-53 improves compatibility with polymers (Al). The permeability of CO₂, N₂, and CH₄ reported in the case of pure cellulose acetate is 16, 1.7, and 1.4 barrers in the CA/NH₂-MIL-53(Al) mixed matrix membrane permeation investigation for CO₂, N₂, and CH₄ done at 3 bar pressure and 25°C temperature. After creating CA/NH₂-MIL-53(Al) MMM, there was a noticeable improvement in selectivity, which was determined as 23.5, 2.3, and 52.6, respectively, for CO₂/CH₄ and CO₂/N₂ [39].

2.2 Graphitic carbon nitride (g-C₃N₄) based mix matrix membranes:

While high-selectivity membranes make it difficult for gas molecules to permeate them, reducing their permeability, high-permeability membranes do not separate gas molecules from one another more effectively. The membranes can be modified using inorganic fillers like zeolite, which is one of the effective solutions to this problem. Modifying the membranes with inorganic fillers like zeolite[40], graphene oxide (GO) [41], and other materials is one of the effective solutions to this problem. GCN nanosheets are becoming more popular for use as a nanofiller in membranes used for gas separation because of their simple and affordable technique of manufacture[42, 43]. Because g-C₃N₄ has a high thermal stability, adding these nanosheets to the membranes improves the thermal stability of the membrane for high-temperature procedures. Additionally, the fractional free volume of the membranes is increased by the introduction of g-C₃N₄ nanosheets[32]. This increases the membrane's permeability by giving gas molecules greater room to pass through it. Additionally, the g-C₃N₄'s molecular sieving ability can increase the selectivity of the membranes for gas separation. In other words, smaller molecules can penetrate membranes more easily because of the presence of g-C₃N₄, whereas larger molecules must travel a longer, more complicated route[44]. The membrane's selectivity consequently gets better. Although g-C₃N₄ offers a significant potential to improve membrane-based gas separation techniques, there are few relevant studies. The production of superior g-C₃N₄ gas separation membranes is inhibited by the difficulty in obtaining the structural integrity of the 2D g-C₃N₄ plane through the delamination of bulky g-C₃N₄ into nanosheets. In order to guard and correct various flaws in g-C₃N₄ nanosheets during the production of gas separation membranes, flexible GO nanoplates with a lot of functional groups were used.

Table 2. 1 Literature review of g-C₃N₄ nanosheets mixed matrix membranes

Serial no.	Polymer	Filler	Permeability and selectivity	Reference
1	Matrimid	Protonated g-C ₃ N ₄	Permeability (CO ₂): 7.69 Barrer Selectivity (CO ₂ /CH ₄): 49.6	[45]
2	Pebax	g-C ₃ N ₄	Permeability (CO ₂): 33.3 GPU Selectivity (CO ₂ /N ₂): 67	[44]
3	PIM-1	g-C ₃ N ₄	Permeability (H ₂): 3830 Barrer Selectivity (H ₂ /N ₂): 10.8	[32]
4	PES support	ZIF-8/ g-C ₃ N ₄ / Chitosan	Permeability (CO ₂): 1.83×10^{-8} mol/m ² s Pa Selectivity (CO ₂ /CH ₄): 17.8	[46]
5	Anodic aluminum oxide substrate	GO/ g-C ₃ N ₄	H ₂ permeance: 2.16×10^{-7} mol/m ² s Pa, Selectivity (H ₂ /CO ₂): 39.2	[47]

Chapter 3

Experimental Methods

3.1 Materials used:

- Cellulose Acetate (CA) (Mw-50,000) from Sigma Aldrich, UK
- Tetrahydrofuran (THF) +99% Pure from Sigma Aldrich, UK
- Another research participant in the study group provided graphitic carbon nitride (g-C₃N₄) nanosheets as-prepared form.
- Gas permeation testing of CO₂ and CH₄ acquired from Linde Chemicals with 99.99% purity of single gas respectively.

3.2 Synthesis of pure CA membrane:

The solution casting process was used to create pure cellulose acetate membrane. In this instance, 1 g of CA was dissolved in 10 ml of Tetra Hydro-Furan (THF) solvent to create a 10% solution, and the mixture was left to stir throughout the night. After the homogenized solution has formed, pour it onto a petri dish and give it 24 hours to evaporate at room temperature. Place petri dish in vacuum oven for 4-5 hours at 40°C to completely remove solvent. a pure CA membrane that was manufactured with a membrane thickness of about 26 μm.

3.3 Fabrication of Mixed Matrix Membranes:

A mixed matrix membrane improves a gas's permeability and selectivity from a group of gases while also adding mechanical stability. Graphitic carbon nitride (g-C₃N₄) nanosheets was dissolved in several vials of THF at different weight percentages ranging from 0.5-1.5 wt%, and CA was likewise dissolved in a separate vial of THF using magnetic stirring for 24 hours. After thoroughly combining g-C₃N₄ nanosheets with THF, add this mixture to the already dissolved CA+THF solution and stirred

again for 24 hours. After 24 hours stirring, the hybrid solution is sonicated for two hours to ensure that nanosheets are thoroughly and uniformly dispersed throughout the CA matrix. Then the hybrid polymer-filler solution was casted on petri dish. Give the solvent 24 hours to evaporate, and for total solvent removal, place the petri dish in a vacuum oven for 4 to 5 hours at 40°C. Membrane thickness of the produced CA/ g-C₃N₄ nanosheets mixed matrix membrane is 26-28 μm.

Many membrane samples were synthesized, and gas permeation testing was performed by passing CO₂ and CH₄ gases through these sample membranes. Infrared Fourier Transform (FT-IR) spectroscopy, scanning electron microscopy (SEM), X-ray Diffraction (XRD), and ultimate tensile testing studies are then used to characterize the membranes.

3.4 Testing and Characterization

3.4.1 Scanning Electron Microscopy (SEM)

Utilizing a scanning electron microscope (SEM), examination was done to look at the morphology and physical makeup of the membrane matrix at various resolutions (JSM-6490, Joel Japan). This research provided detailed information on the morphology of the membrane surface, pore size geometry, and surface and cross-sectional morphology. The membrane samples were created on copper stubs before being coated with gold using a sputter technique[48, 49].

3.4.1.1 Components of SEM

SEM consists of following components.

- Electron generating source
- Magnetic lenses
- Sample Stage
- Scanning system
- Electron detector
- Display (TV Scanner)
- Vacuum system
- Electronic control

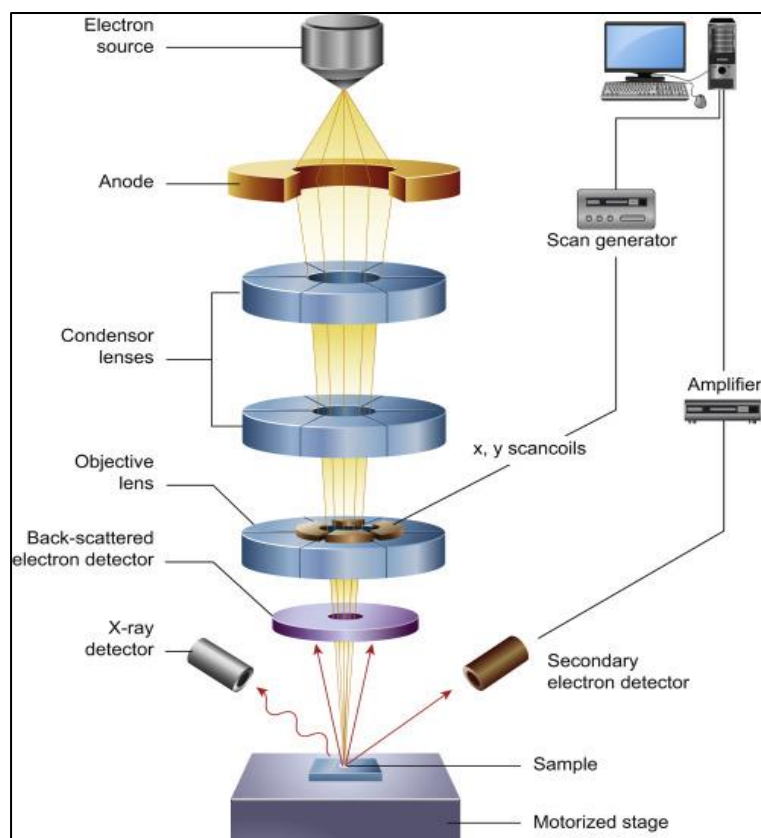


Figure 3. 1 Schematic diagram of scanning electron microscopy (SEM) machine [48, 49]

3.4.1.2 SEM Working Principles

When a high-energy electron beam struck a membrane sample, it dispersed into a variety of signals, as seen in Figure 3.1. which concentrated on the material's surface. The electron detector captured signals produced by the interaction of membrane samples with electron beams. In order to assess the shape of membranes, these signals were then appropriately examined. The samples were examined at various magnifications ranging from X500 to X20000 using a 10 KV voltage. SEM is regarded as a non-destructive analytical technology because samples are not damaged throughout the procedure[48, 49].

3.4.2 Fourier transform Infrared (FT-IR) Spectroscopy

Fourier transform infrared (FT-IR) spectroscopy is an analytical technique carried out to evaluate the presence of function group in organic compounds and its modes as represented in Figure 3.2 and 3.3. Which also includes, detecting the chemical bond type in molecules, molecular structure of membrane samples. For this characterization,

Perkin-Elmer spectrum 100 FT-IR spectrometer was used at a range of 4000 – 400 cm^{-1} wave number with a resolution of 4 cm^{-1} [50, 51].

3.4.2.1 Components of FT-IR Spectrometer

FT-IR spectrometer consist of the following component.

- Infrared (IR) source
- Beam Splitter
- Fixed and movable mirrors
- Sample cell
- Detector

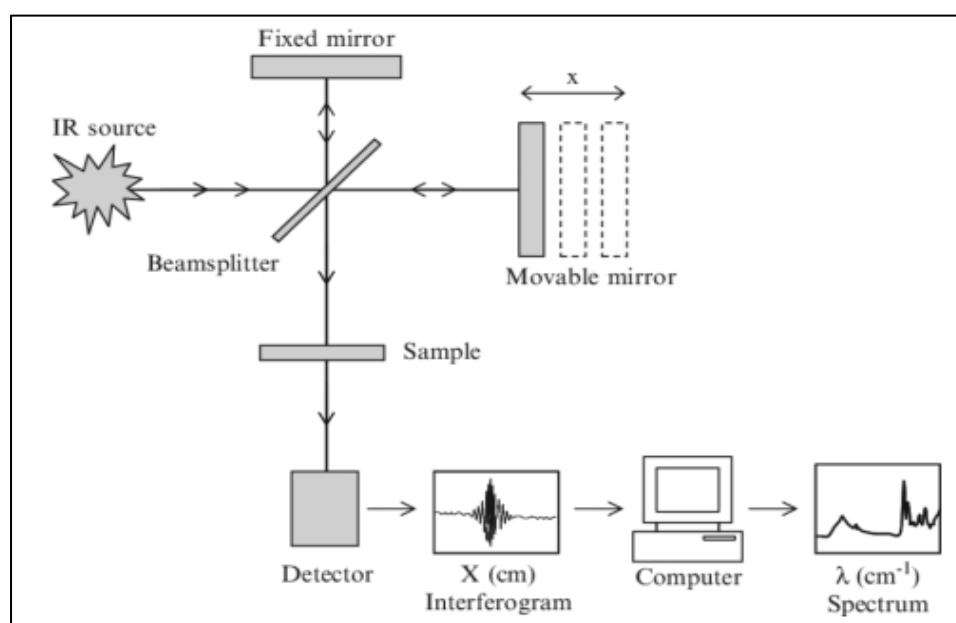


Figure 3. 2 Schematic diagram of Fourier Transform Infrared (FT-IR) Spectrometer

3.4.2.2 Working Principles

As shown in Figure 3.2, an IR radiation was produced by an IR source in the FT-IR spectrometer, which was subsequently absorbed by the substance, causing the molecules' energy state to rise from a lower energy level to an excited energy state. The molecules acquired a higher vibrational state by this method. According on the wavelength of the radiation received, a certain amount of energy is required to move the molecules into that higher state. Each specific functional group found in a molecule absorbs light at a particular wavelength. This resulted in a spectra peak known as the functional group's fingerprint. A spectrum of those specific molecules is created when all the distinguishing peaks of the various functional groups present in a material are merged; this spectrum is known as the FT- IR spectrum[50, 51].

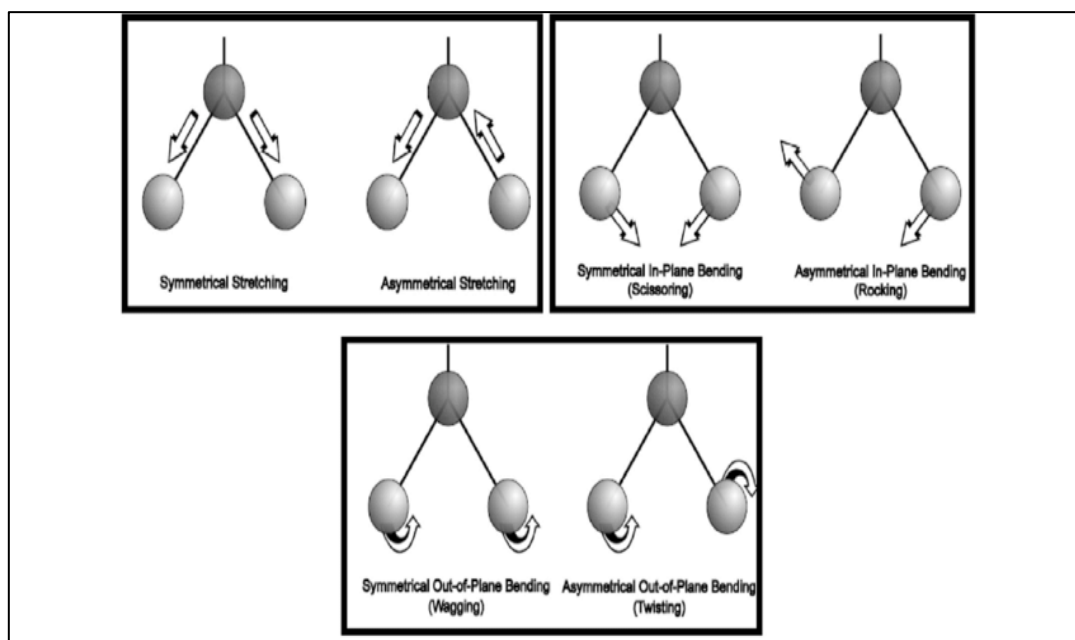


Figure 3. 3 Different modes of molecular vibration in FT-IR (stretching and bending)

3.4.3 X-Ray Diffraction (XRD)

The crystallinity of the material was assessed using the XRD characterisation technique (membranes). The phase identity, purity, crystal structure, and crystallinity of membrane are all thoroughly described by XRD[52].

3.4.3.1 Components of XRD

XRD consist of the following components.

- X-Ray Tube
- Sample holder
- Detector

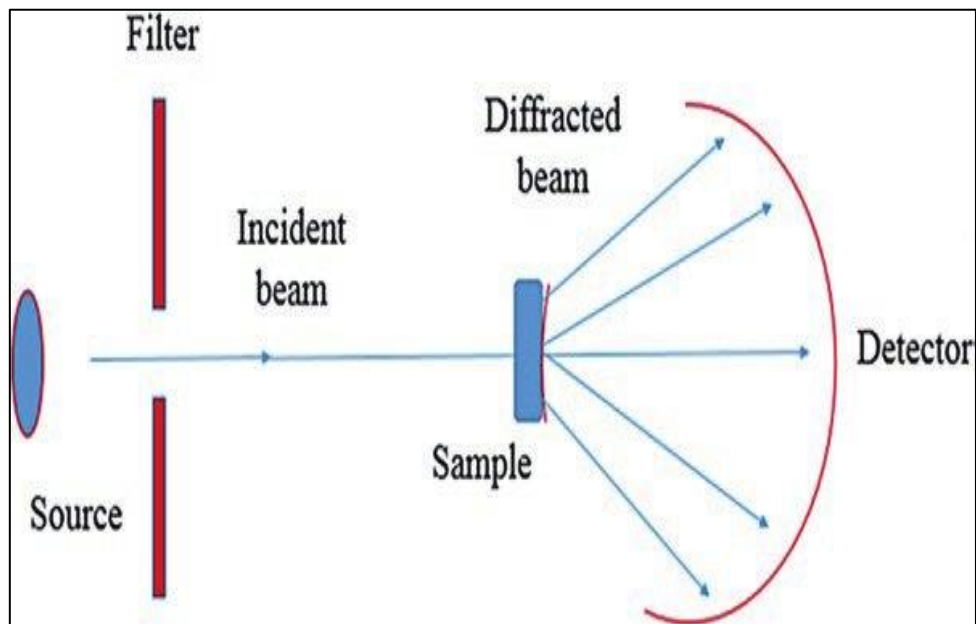


Figure 3. 4 Schematic diagram of X-Ray Diffraction characterization

3.4.3.2 Working Principles

The principles of how XRD works are shown in Figure 3.4. Monochromatic X-ray tubes are used to create rays. Collimator is used to pass through X-rays. These rays are then focused and pointed in the direction of the sample stage. When X-rays interact with the test samples and some of the rays get diffracted, a constructive interference is created. This applied the criteria of Bragg's Law ($n = 2d \sin$) shown in Figure 3.5. It links the diffracted angle and sample lattice spacing to electromagnetic radiation wavelength. It is possible to gauge the crystal size using

Debye-equation. Scherer's Each crystal has a distinct fingerprint pattern that can be used to identify it[52].

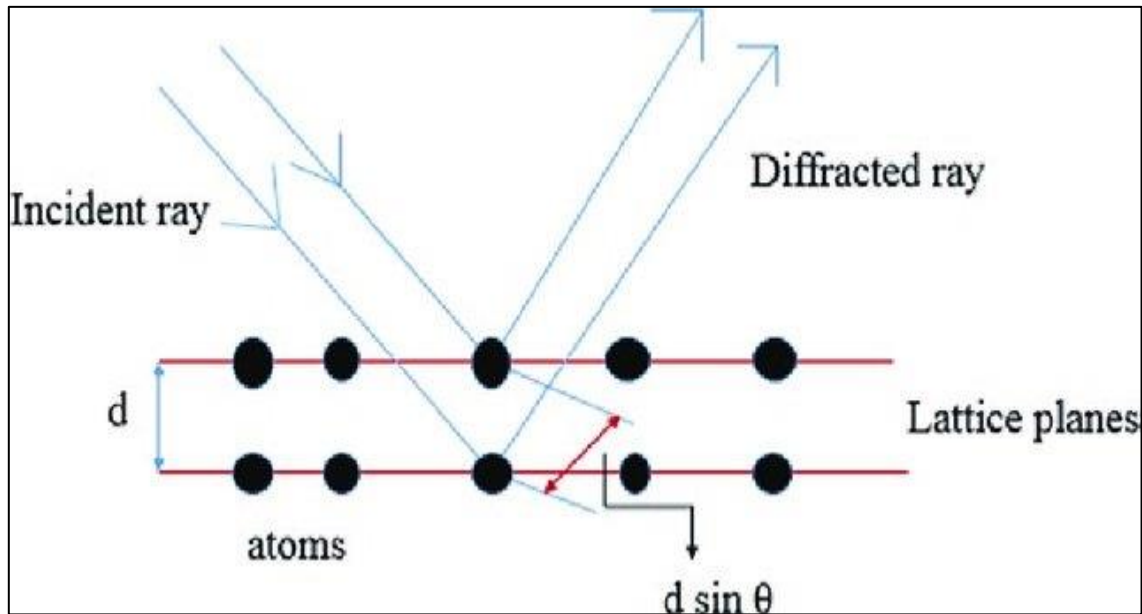


Figure 3. 5 Bragg's Law X-Ray Diffraction system

3.4.4 Gas Permeation Testing

To learn more about the perm-selective properties of the membranes, gas permeation testing and analysis were done. The gas permeation of membrane sample was assessed for this purpose using the PHILOS-Korea gas permeation testing system, as shown in Figure 3.6. The standard deviation and random errors were removed after testing three samples of each membrane[53].

3.4.4.1 Components of Gas Permeation Testing Rig

The following are the components of gas permeation testing rigs.

- Membrane Cell
- Flow regulators
- Bubble flow meter
- Flow valves
- Vent tube

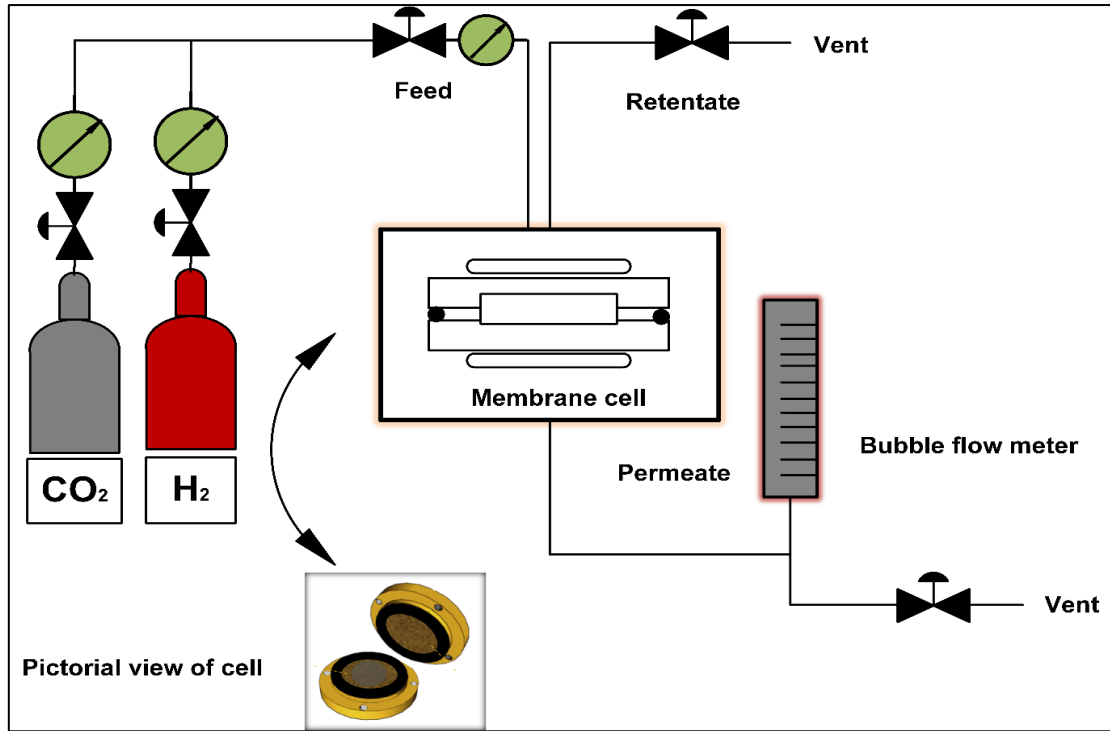


Figure 3. 6 Gas permeation testing system rig

3.4.4.2 Working Principle of Gas Permeation Testing Rig

A membrane cell with two porous ceramic discs was used to hold the samples, which were then reduced to a size of 8.0 cm² and placed within. Gases such as methane (CH₄) and carbon dioxide (CO₂) were employed as feed gases in this investigation. Using a gas flow metre, also known as a bubble flow metre, the findings of the permeation analysis test were recorded and calculated at a gauge pressure range of 2.0 to 5.0 bars, constant volume, and a constant temperature of 25 °C. The solution-diffusion mechanism is used to characterise the gas permeation, and the results of the following equations are used to estimate the process[53].

$$P_i = \frac{Q\Delta L}{A\Delta P} \quad \text{Eq (4.2)}$$

$$P = S \times D \quad \text{Eq (4.3)}$$

$$\alpha_{i/j} = \frac{P(i)}{P(j)} \quad \text{Eq (4.4)}$$

3.4.5 Mechanical Testing

Tensile strength testing and elongation at break percent were two mechanical tests performed on membrane samples to look into their various mechanical properties. Three samples of each membrane were used to determine the mechanical characteristics, and the standard deviation was estimated to remove random errors[53, 54].

3.4.5.1 Components of Ultimate Tensile Testing Machine (UTM)

The following are the components of the ultimate tensile testing machine (UTM).

- Screw Column
- Adjustable upper crosshead
- Wedge Grips
- Adjustable Lower Crosshead
- Base and encoder assembly

3.4.5.2 Working Principle of Ultimate Tensile Testing Machine (UTM)

The ratio of the highest stress a material can withstand before permanently deforming the membrane's physical structure to its strain can be used to assess that material's maximum tensile strength. The type of the materials glassy or rubbery determines their level of strength as shown in figure 3.7. The end point of each curve in this diagram illustrates how the brittle (glassy) materials exhibit great tensile strength while only exhibiting minor strain. In contrast, the rubbery material that is more flexible exhibits a high strain but a significantly lower tensile strength. The mechanical properties of the membranes are ascertained for this purpose using the UTM SHUMADZU AGS-X Plus Japan machine, as shown in Figure 3.8. The mechanical testing was carried out at an elongation rate of 1 mm/min after the membrane samples were cut in accordance with ASTM standard D882-02.

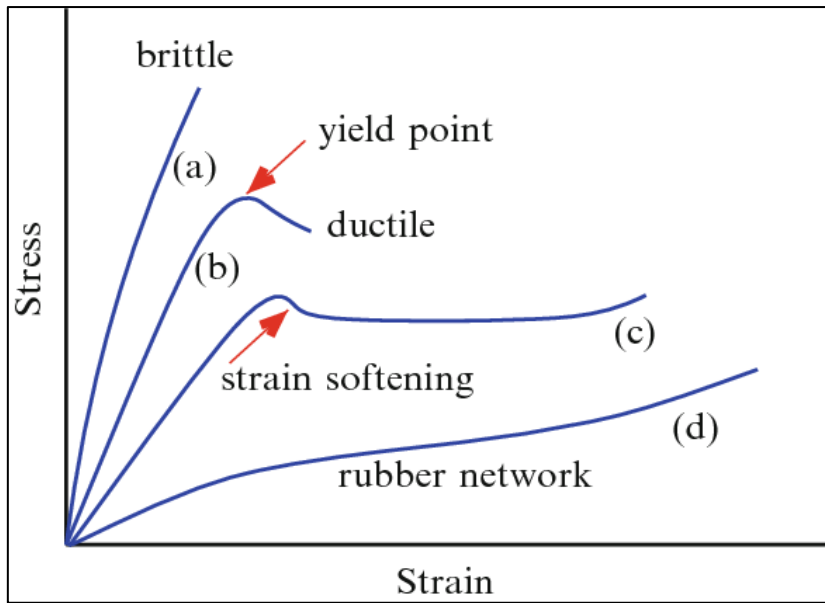


Figure 3. 7 stress-strain behavior of several classes of materials

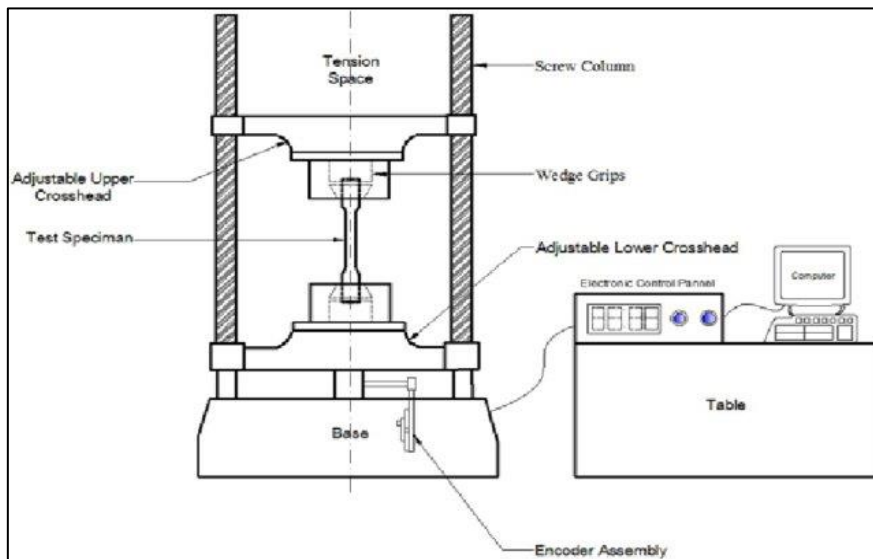


Figure 3. 8 Schematic diagram of ultimate tensile testing system

Chapter 4

Results and Discussion

4.1 Characterization techniques:

The membranes' various properties have been examined using a variety of characterisation techniques. The following are the many methods used for characterization:

- The analysis of the various functional groups found in the membrane structure using Fourier Transform Infra-Red (FT-IR) Spectroscopy.
- Scanning electron microscopy, which is used to examine and assess the membrane's pore structure and surface shape.
- Tensile testing analysis, which measures the membranes' mechanical strength.
- XRD analysis carried out to analyze the crystallinity of the membranes.
- Gas permeation testing was utilized to study permeance and selective nature of different gases permeating through the membranes.

4.1.1 Fourier Transform Infra-Red (FT-IR) Spectroscopy:

The presence of functional groups, chemical linkages, and interactions between the filler and polymer matrix were confirmed by FTIR analysis of all membrane samples, which is shown in Figure 4.1. The intermolecularly bound hydroxy group (O-H) with a bell-shaped unique structure was represented by the absorption FT-IR band about 3498 cm^{-1} in the FT-IR spectra of the (CA) membrane. The stretching of the acetate group, which produced the FT-IR absorption peaks at about 1240 cm^{-1} and 1742 cm^{-1} , is attributed to the (C-C-O) and (C=O) stretchings. FT-IR absorption peaks at wavenumbers of 2959 cm^{-1} and 2883 cm^{-1} distinguish between the symmetric and asymmetric stretching of $\text{C}_{\text{sp}^3}\text{H}$ (methyl groups). The asymmetric and symmetric deformation peaks for $\text{C}_{\text{sp}^3}\text{H}$, however, are found at 1430 cm^{-1} and 1378 cm^{-1} , respectively. The peak at 1062 cm^{-1} is attributed to $-\text{CH}_2\text{-OH}$ group (C-O) stretching. The past research strongly supports all of the sample CA peaks[55].

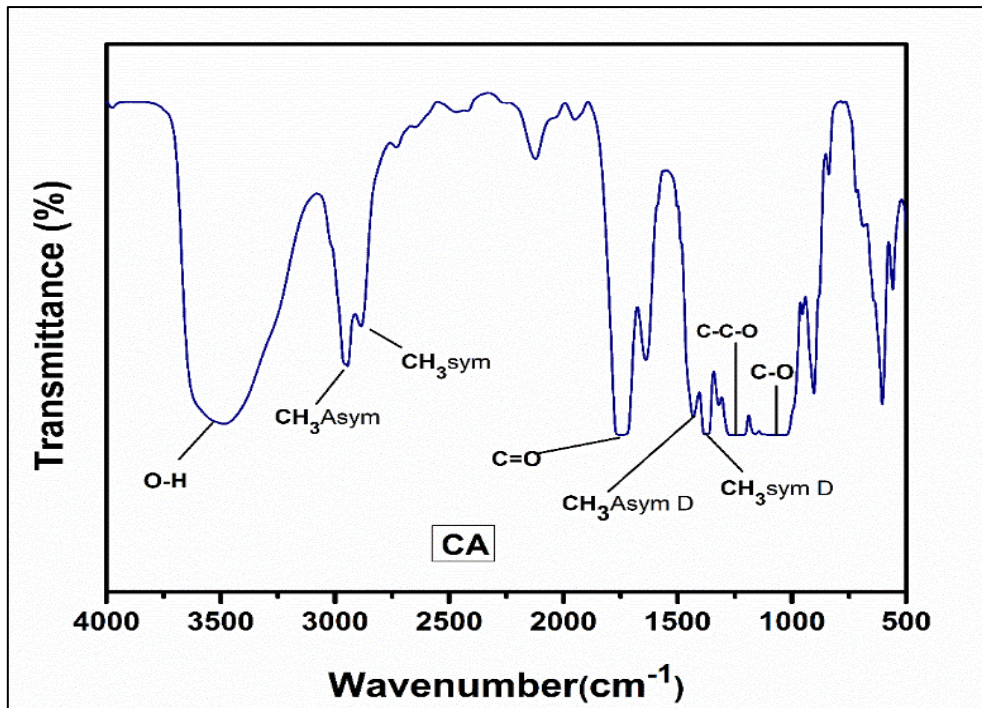


Figure 4. 1 Pure CA membrane's FTIR spectrum

After incorporation of g-C₃N₄ nanosheets in CA matrix, due to the physical interaction between CA and g-C₃N₄ through hydrogen bonding, an intermolecular force attraction, as can be shown in figure 4.2, no new peak did not develop in the MMMs of CA/g-C₃N₄ (0%, 0.5%, 1.0%, and 1.5% (w/w)). Peaks from CA and g-C₃N₄ are the sources of the peaks in the FT-IR spectrum of mixed matrix membranes. In CA/g-C₃N₄ MMMs, the following absorption bands can be observed: 3432, 2942, 2473, 1743, 1377, 906 and 810 cm⁻¹ [56].

As the loading of g-C₃N₄ increased from 1 to 1.5 wt% the characteristic peaks of 810 cm⁻¹ is observed which is related to the s-tria-zine ring mode[57]. The peak observed at 3432 cm⁻¹ confirms the hydroxyl group presence in the MMM. A small variation in the degree of stretching of the hydroxyl groups was brought on by the addition of g-C₃N₄. Peak repositioning and a decline in relative intensity indicated the development of potent interfacial contacts between residual -NH or -NH₂ of g-C₃N₄ and -OH groups of CA, which result from hydrogen bonding.

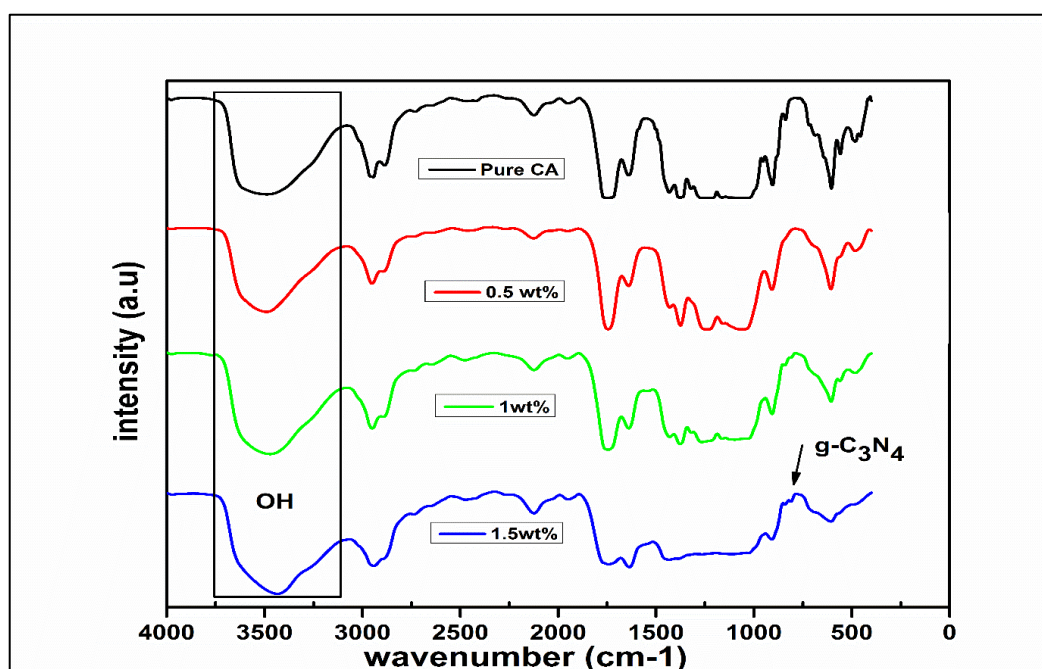


Figure 4. 2 FTIR spectrum of CA/g-C₃N₄ MMMs

The occurrence of asymmetric and symmetric methyl groups (CH₃) in the polymer phase (CA) of all the MMMs was confirmed by the appearance of peaks at 2942 and 2473 cm⁻¹. The presence of the carbonyl group (C=O) in the polymer phase (CA) of all the MMMs was confirmed by a peak at 1743 cm⁻¹. The presence of the peaks in the 1 and 1.5 wt% loadings of g-C₃N₄ nanosheets in CA/g-C₃N₄ MMM's depicts the agglomeration of the nanosheets in the polymer matrix.

4.1.2 Mechanical Testing:

The mechanical characteristics of cellulose acetate membranes combined with graphitic carbon nitride nanosheets were examined using tensile stress-strain testing. The UTM machine was used to examine the mechanical characteristics. Tensile strength and the length of a membrane before breaking are among the qualities that are investigated. In general, the force used to test composite membranes was transferred from the polymeric matrix to the inorganic portion, specifically the graphitic carbon nitride nanosheets. Consequently, the nature, intrinsic interactions, and extrinsic interactions of the nanoparticles strongly influence the properties of membranes combined with inorganic fillers[58, 59].

The ultimate tensile strength of each membrane sample is determined at an elongation rate of 0.5 mm/min, as illustrated in Figure 4.2. After multiple experiments with both high and low elongation rates ranging from 0.1 to 1 mm/min, the elongation value is chosen. Tensile strength is much more than it should be when the elongation rate is too low, whereas it is much lower than expected when the elongation rate is too high. The membrane strength will only be more correctly reflected with a moderate value of elongation rate, such as 1 mm/min.

Figure 4.3 shows that once the experiment is completed and the elongation rate is determined, adding modest amounts of GCN, like 0.5%, causes the tensile strength to rise to a very high number which is 81.66 MPa. Strong interfacial contacts between g-C₃N₄ and CA and homogeneous dispersion of g-C₃N₄ were credited with the increase in strength.

The tensile strength of the membranes, however, falls even lower than that of the membrane with no GCN nanosheets integrated in its matrix when the amount of GCN nanosheets is increased above 1.0%. This was explained by the aggregation of g-C₃N₄ nanosheets, which caused the lamellar structure to degrade[59].

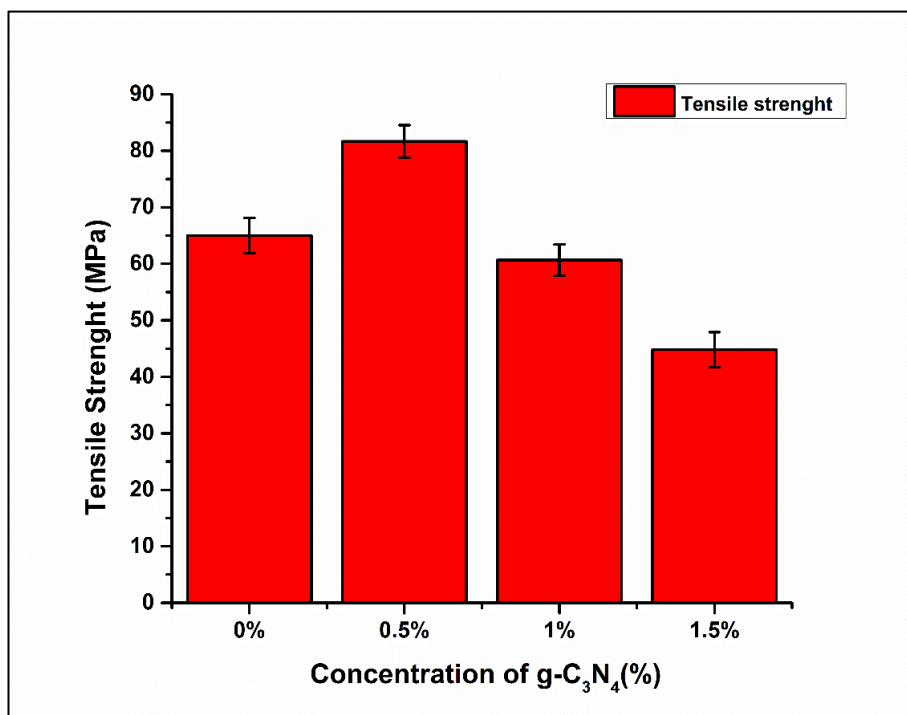


Figure 4. 3 Ultimate tensile strength for membrane samples with g-C₃N₄ loading of 0%, 0.5%, 1.0%, and 1.5%

4.1.3 Scanning Electron microscopy (SEM) analysis:

Scanning Electron Microscopy (SEM) analysis was used to test the various membrane samples, as seen in Figure 4.4 and Figure 4.5. Magnifications of 500x, 1000x, 2500x, 5000x, and 10000x were used to analyse each sample. The entire dense and defect-free membrane is created, as shown by the surface and cross-sectional images of pure CA membrane. White dots scattered across the surface of each of these samples' flawlessly dense formations indicated the presence of GCN nanosheet particles. Our analyses revealed that the structure and morphology of the membrane's perforations are not significantly changed by the addition of more nanosheets. Also, the distribution of the white spots demonstrates the appropriate dispersion of the GCN nanosheets within the membrane which is the result of ultrasonication[31]. It contributes to the membranes' excellent performance in terms of gas separation. SEM examinations are performed after the membranes are tested for their ability to restrict the passage of gases, tracks can be observed in the polymer structure, which are a result of the effect of permeation testing on the membranes.

In addition, microcavities can be identified in the cross-sectional pictures of GCN nanosheets hybrid membranes, especially at 1.0 and 1.5 wt% loading of GCN nanosheets. These microcavities indicated that GCN and CA were interacting strongly at the interface. However, it was not as powerful as needed to segregate these aggregates. Moreover, the creation of microcavities may have been caused by the concentration of stress at the interface and the rupturing of membranes under liquid nitrogen[60]. The selectivity and mechanical strength of the membrane would also be decreased by the agglomeration of g-C₃N₄ nanosheets, especially at higher loadings of about 1.5 wt%, which will be covered in the section on gas permeability[58, 61].

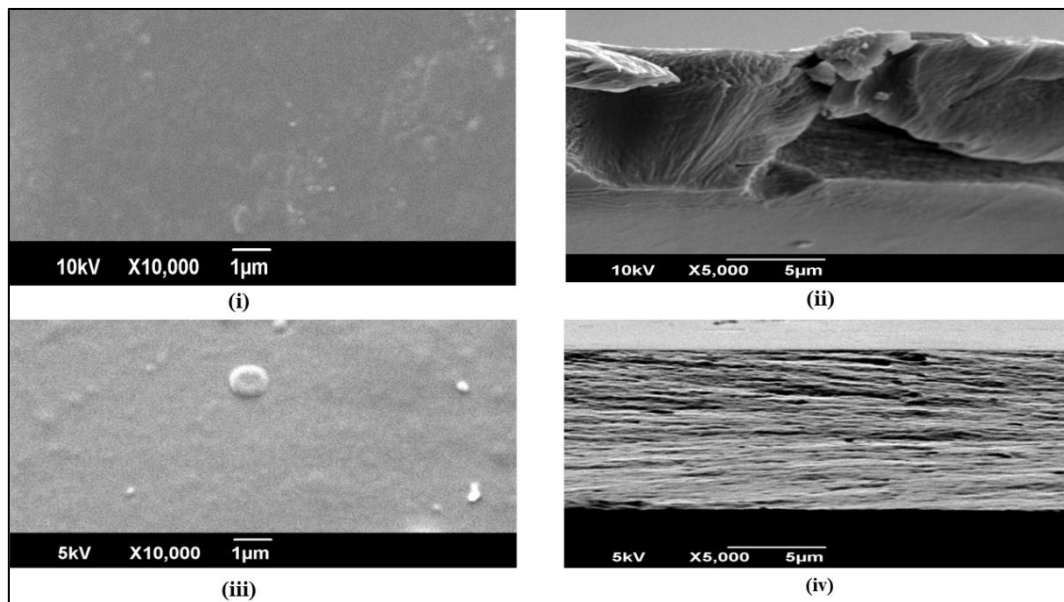


Figure 4. 4 SEM images of membrane samples (i)Pure CA surface (ii) Pure CA cross-section (iii)surface of g-C₃N₄/CA 0.5 wt% (iv) Cross surface of g-C₃N₄/CA 0.5 wt%

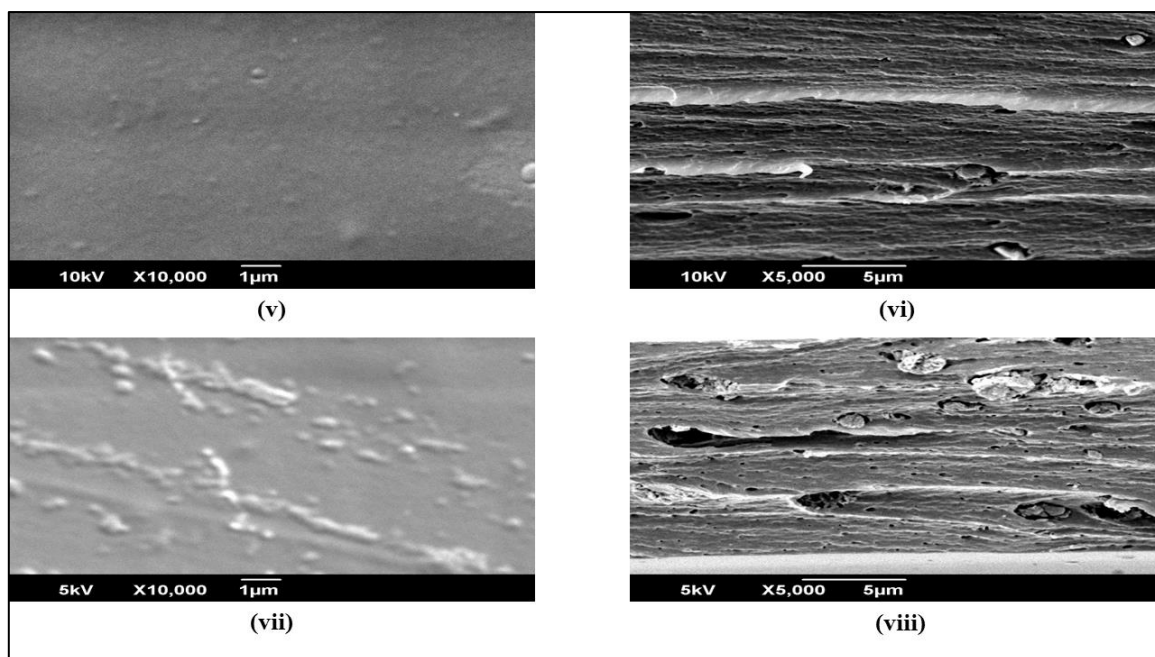


Figure 4. 5 SEM images of membrane samples (v) surface of g-C₃N₄/CA 1 wt% (vi) cross-section of g-C₃N₄/CA 1 wt% (vii) surface of g-C₃N₄/CA 1.5 wt% (viii) cross-section of g-C₃N₄/CA 1.5 wt%

4.1.4 XRD Analysis:

X-ray diffraction (XRD) is a powerful analytical technique used for the identification and quantification of crystalline materials in a sample. The XRD analysis of CA-MMMs with the incorporation of g-C₃N₄ nanosheets provides important information about the structure and morphology of the composite membrane. The crystallinity and purity of the manufactured membrane samples, as well as the polymer chain packing, were all described by the XRD pattern. The analysis also helps in determining the degree of interaction between the nanosheets and the polymer matrix. This also includes the sample of pure CA membrane, pure GCN nanosheets, and mixed matrix membranes that contain both GCN and CA. These XRD analyses were performed at a scan rate of 0.04°/s between the 2 θ angles of 5 and 40°.

Amorphous and semi-crystalline phases make up the polymer structure. Amorphous phase polymer chains are randomly arranged and exhibit broad, low intensity peaks. Contrarily, polymer chains are neatly aligned in crystals, resulting in crystal peaks that are well defined.

As shown in figure 4.6 (i), two large diffuse amorphous peaks with diffraction angles of 2 θ = 10° and 17° were found in the XRD pattern of CA. Semi-crystalline polymers include CA. Strong intermolecular contact (hydrogen bonding) between the acetyl and hydroxyl groups is the cause of its low crystallinity.

Figure 4.6 (ii) shows the XRD of graphitic carbon nitride nanosheets, two distinct diffraction peaks may be seen on it. The interlayer stacking of conjugated aromatic planes, with an index of (002) and a d-spacing of 0.325 nm, is responsible for the prominent peak detected at 27.5°. Moreover, the faint peak at roughly 13° (d-spacing = 0.693) is a defining feature of the tri-s-triazine units' in-plane structural packing pattern[62, 63].

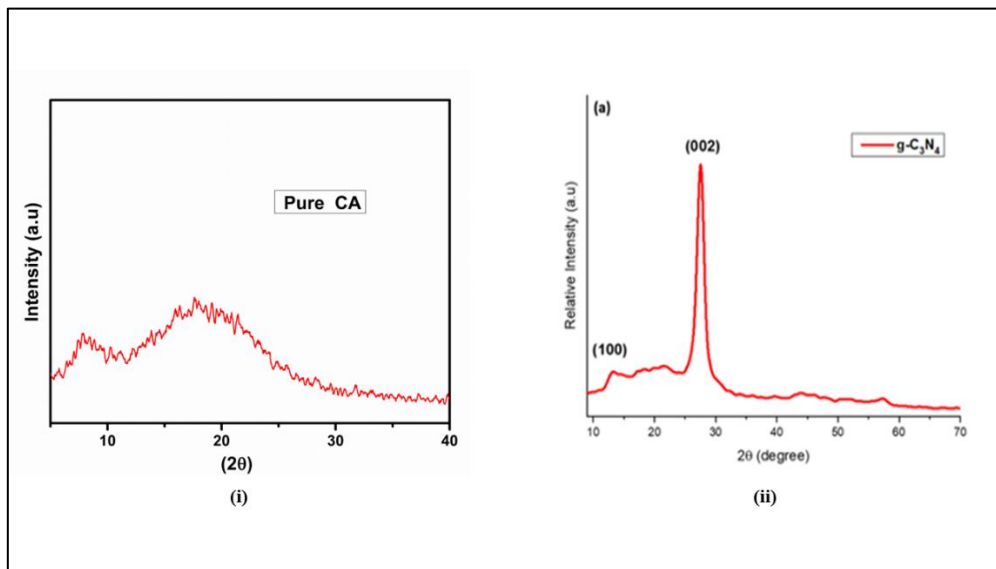


Figure 4. 6 XRD pattern of (i) pure CA and (ii) g-C₃N₄ nanosheets

XRD pattern of different wt.% (0.5, 1.0 and 1.5) loadings of GCN in CA/g-C₃N₄ mixed matrix membranes is demonstrated in figure 4.7. we investigate effect these loadings on the crystal structure of these mixed matrix membranes. The addition of g-C₃N₄ has a disruptive effect on the crystalline structure of CA, as evidenced by the decrease in the intensity peak of CA at 17°. The development of intermolecular hydrogen bonds between CA and GCN nanosheets may be the cause of this disruptive effect. The XRD results suggest that the addition of g-C₃N₄ disrupt the crystalline structure of CA leading to a decrease in the degree of crystallinity of the mixed matrix membrane, which may lead to an increase in the free volume and facilitate the diffusion of gas molecules.

No prominent peak of GCN nanosheets was observed for the 0.5 and 1.0wt % loadings in the XRD pattern. This illustrates how nanosheets were successfully exfoliated and uniformly distributed throughout the polymer matrix. As loading of GCN increases to 1.5wt% the

prominent peak of the g-C₃N₄ is detected at 27.5° which indicates the agglomeration of the nanosheets started in the polymeric membrane. Which is confirmed by the SEM Image from figure 4.5 (vii). Therefore, the incorporation of g-C₃N₄ into the mixed matrix membrane can be a promising approach to enhance its gas separation performance[64].

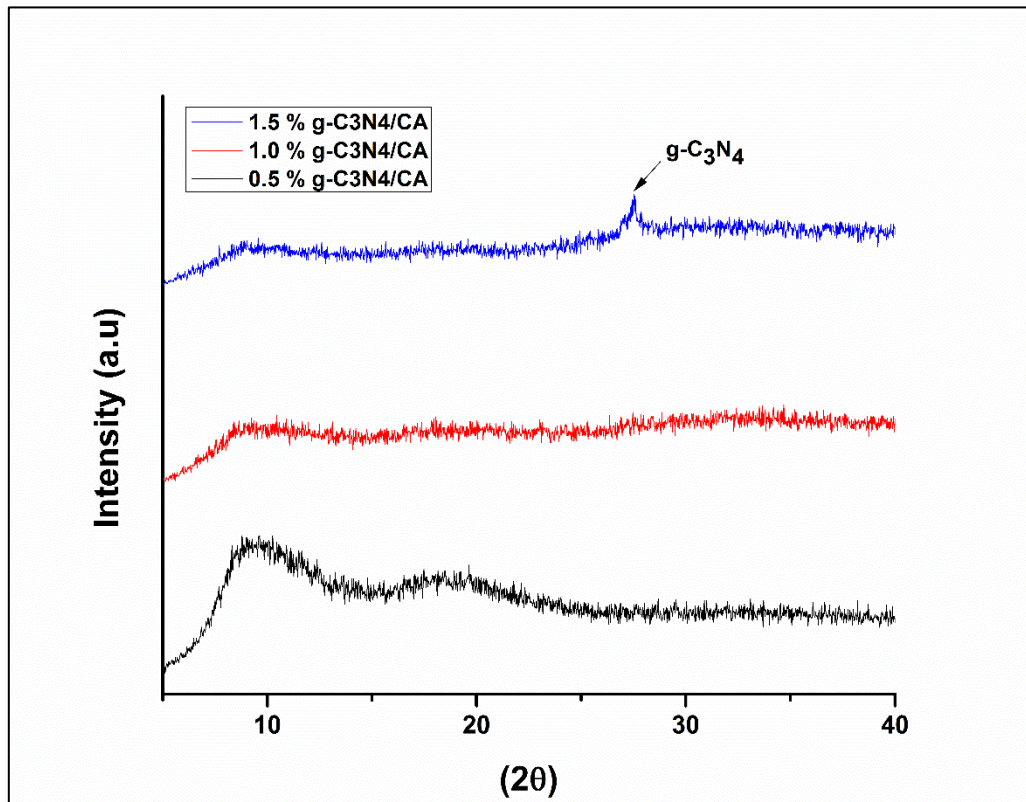


Figure 4. 7 XRD pattern of g-C₃N₄/CA MMMs with different wt.%

4.1.5 Gas Permeation Testing:

Using the stainless steel gas permeation rig and adjusting pressures of 2, 3 ,4 and 5 bars individually, single gas tests were conducted to evaluate the permeation of CA/ g-C₃N₄ mixed matrix membranes containing (0.5wt%), (1.0wt%) and (1.5 wt%). The following table 4.1 provides a summary of the permeability results of mixed matrix membranes. Permeability of CO₂ with pressure. Permeability of CH₄ with pressure

Table 4.1 Gas permeation testing:

Membrane Samples	Permeability of CO ₂ (Barrer)	Permeability of CH ₄ (Barrer)	Selectivity of CO ₂ / CH ₄	Pressure (bars)
Pure CA	32.44	16	2.03	2
Pure CA	34.23	18.74	1.83	3
Pure CA	38.5	21.5	1.79	4
Pure CA	41.34	24.3	1.70	5
CA/g-C ₃ N ₄ 0.5 wt%	78.05	28.62	2.73	2
CA/g-C ₃ N ₄ 0.5 wt%	125.81	48.56	2.59	3
CA/g-C ₃ N ₄ 0.5 wt%	140.26	56.57	2.48	4
CA/g-C ₃ N ₄ 0.5 wt%	150.73	63.14	2.39	5
CA/g-C ₃ N ₄ 1.0 wt%	112.75	53.36	2.11	2
CA/g-C ₃ N ₄ 1.0 wt%	140.93	70.56	1.99	3
CA/g-C ₃ N ₄ 1.0 wt%	181.20	98.23	1.84	4
CA/g-C ₃ N ₄ 1.0 wt%	213.63	120.69	1.77	5
CA/g-C ₃ N ₄ 1.5 wt%	109.11	67.25	1.39	2
CA/g-C ₃ N ₄ 1.5 wt%	130.13	99.27	1.31	3
CA/g-C ₃ N ₄ 1.5 wt%	149.23	128.26	1.16	4
CA/g-C ₃ N ₄ 1.5 wt%	162.36	145.11	1.12	5

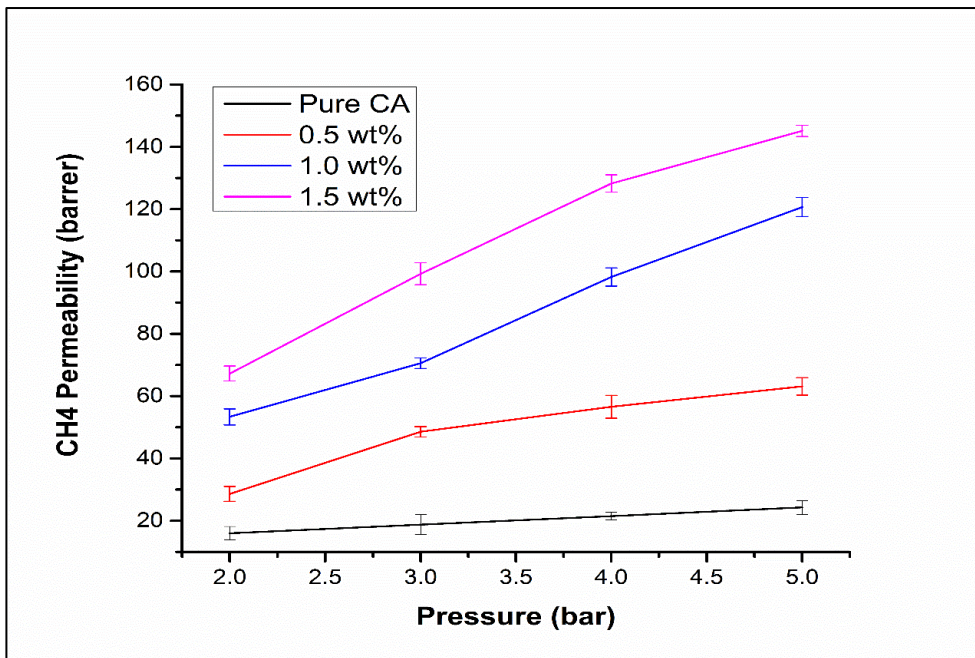


Figure 4.8 a Permeability of CH₄ with pressure

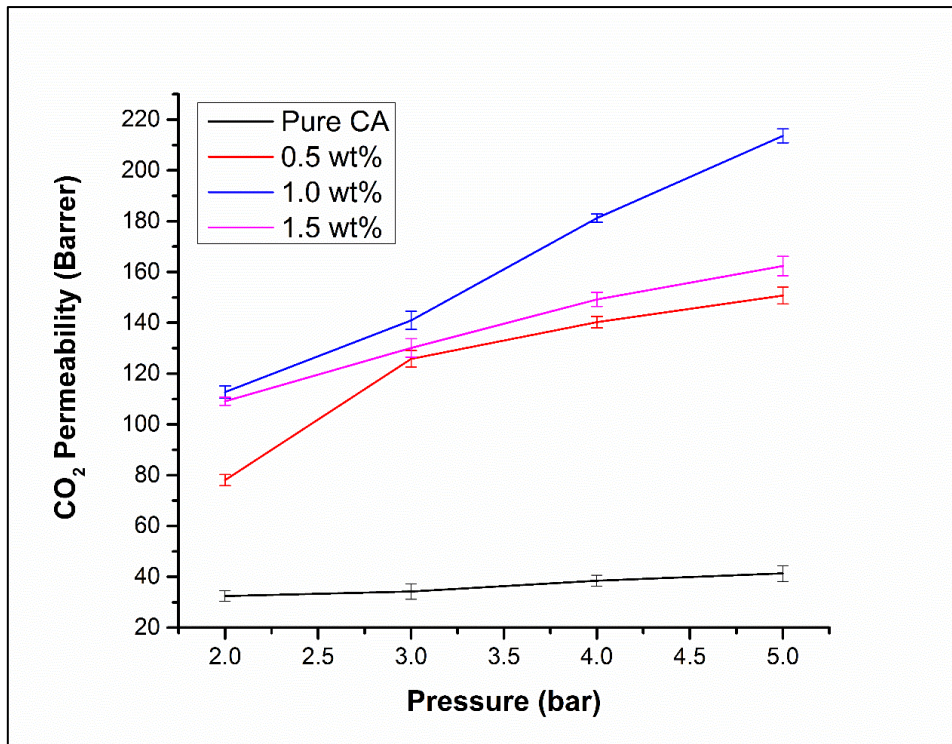


Figure 4.8 b Permeability of CO₂ with pressure

The impact of pressure on the permeability of CO₂ and CH₄ is depicted in Figures 4.8 (a) and 4.8 (b). Both gases become more permeable as the pressure rises. There are two reasons why this can be the case. i) Total free volume within the polymeric membrane rises as pressure increases due to polymer chain distress, which causes an increase in the diffusion coefficient and permeability of gases. ii) The dual sorption model predicts that the concentration of gas species on the surface membrane rises as feed pressure rises, which may have enhanced sorption and diffusion and improved overall gas permeability.

Figure 4.8 (b) depicts the impact of GCN nanosheet concentration on CO₂ permeability and CO₂/CH₄ selectivity. The figure shows that, in comparison to a pristine CA membrane, the permeability of CO₂ increases as the concentration of GCN particles increases. At a loading of 1wt% GCN nanosheets, the highest permeability of 213.63 Barrer was shown. The strong connection between CO₂ and the OH groups that tend to be present on the surface of GCN nanosheets are one of the causes of the increasing trend in permeability of CO₂ with concentration. The structural freedom of CA backbones is thought to be effectively restricted by the presence of high surface-to-volume g-C₃N₄, which also makes efficient packing of polymer chains more difficult. As a result, more frictional free volume was developed, which led to an increase in permeability[65].

No porosity could be seen in SEM pictures of the CA/g-C₃N₄ hybrid membrane, confirming that the process for gas separation via the membrane is totally dependent on solution diffusion mechanism. Figure 4.9 shows the CH₄ permeability with increment in the concentration of GCN nanosheets which shows the highest permeability of 145.11 Barrer at a loading of 1.5 wt%.

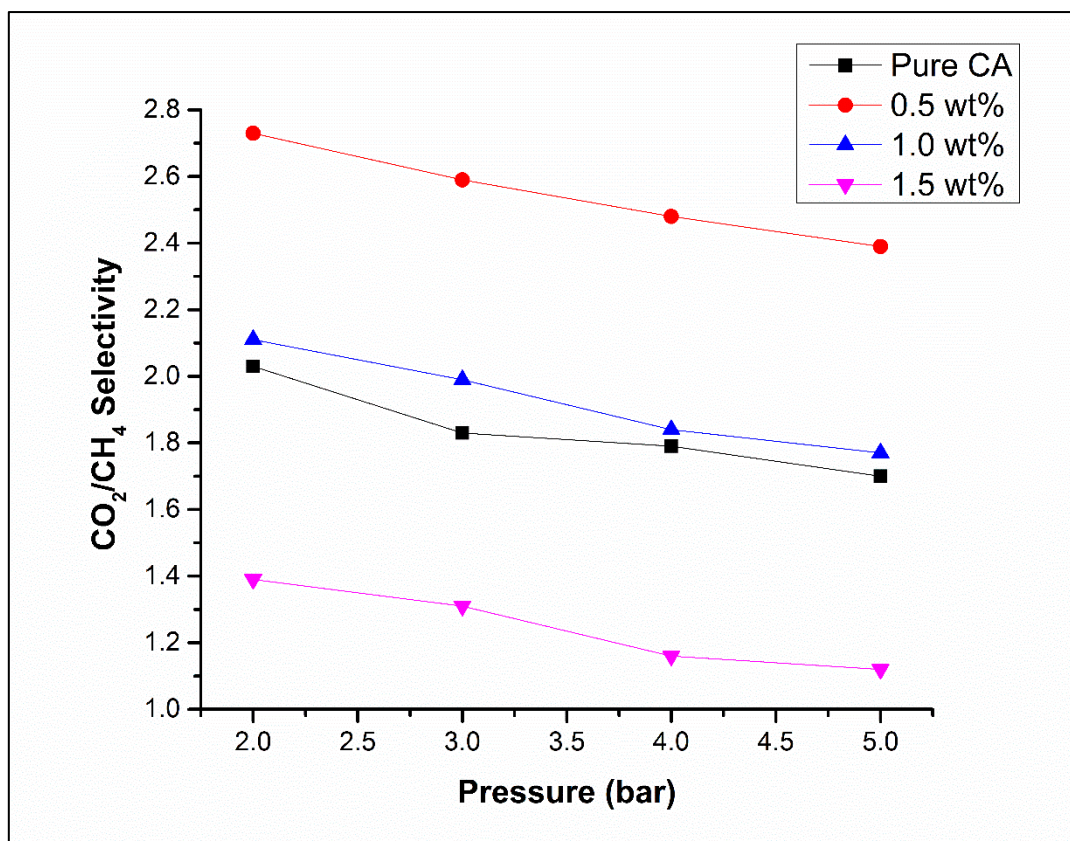


Figure 4.8 a CO_2/CH_4 selectivity of MMM's

The selectivities for CO_2 and CH_4 however, displayed very different patterns. As shown in figure 4.8 (c), CO_2/CH_4 selectivity is increased at a loading of 0.5 wt% of GCN nanosheets which is 2.73. As the loading is increased from 0.5 to 1.5 wt% the selectivity start to decrease gradually. The non-selective voids formed at the intersection of the CA and g- C_3N_4 nanosheets were the main cause of it. In accordance with the trade-off effect, the selectivity towards CO_2 would decrease. Increased permeability of both gases accounts for this reduction in selectivity. This increase in permeability may be brought on by the agglomeration of particles at greater concentrations of up to 1.5wt%.

Conclusion

This work involved the synthesis of mixed matrix membranes using GCN 2D nanosheets as a filler in CA continuous phase. GCN 2 D nanosheet weight percentage was modified for membrane casting, and the impact of pressure and concentration on permeability and selectivity was thoroughly examined. The performance of CO₂/CH₄ single gas separation was assessed for each membrane sample. The best membrane samples were analysed using FTIR, SEM, XRD, and UTM, among other characterisation methods. The confirmation of the essential functional groups was examined using FT-IR. To investigate the morphology and surface characteristics of manufactured membranes, SEM examination was done. The XRD technique was used to investigate structural characteristics. The UTM machine also examined for mechanical properties.

The present work demonstrates that there is only physical interaction between the polymer and nanosheets. This is demonstrated by a careful comparison of FTIR spectra of pure CA and all CA/ g-C₃N₄ mixed matrix membranes. SEM analysis of the membrane samples confirm dense and defect-free membranes are created. Membrane with higher loadings of GCN like 1.5wt % shows the agglomeration of the nanosheets which indicate its reduction in mechanical strength. Maximum CO₂/CH₄ selectivity of 2.73 was obtained for GCN/CA membranes. Permeability of CO₂ was improved to 213.63 Barrer. Also, the results of the tensile strength tests showed that the highest tensile strength for GCN/CA membranes was 81.66 MPa. Which is 25 % more stronger than pure CA membrane. This research suggests that adding GCN 2D nanosheets to CA membranes would improve permeability but have less effect on selectivity. Finally, it is advised that:

- To make the membranes suitable for usage on a broad scale, more research should be done to increase their selectivity.
- Functionalizing the GCN nanosheets can be done to enhance their separation capabilities.

References

- [1]. Now, C.J.-h.w.c.e.m.-c., *Earth's CO₂ home page*. 2015.
- [2]. Liang, F.-Y., et al., *The role of natural gas as a primary fuel in the near future, including comparisons of acquisition, transmission and waste handling costs of as with competitive alternatives*. 2012. **6**(1): p. 1-24.
- [3]. Wasiu, A.B. and M.R. Heikal, *The effect of carbon dioxide content-natural gas on the performance characteristics of engines: a review*. 2012.
- [4]. Darmstadter, J., *Energy and population*. 2004: Resources for the Future Washington.
- [5]. York, R.J.S.s.r., *Demographic trends and energy consumption in European Union Nations, 1960–2025*. 2007. **36**(3): p. 855-872.
- [6]. Owen, N.A., O.R. Inderwildi, and D.A.J.E.p. King, *The status of conventional world oil reserves—Hype or cause for concern?* 2010. **38**(8): p. 4743-4749.
- [7]. Othman, M., et al., *Separability of carbon dioxide from methane using MFI zeolite–silica film deposited on gamma-alumina support*. 2009. **121**(1-3): p. 138-144.
- [8]. Yang, H., et al., *Progress in carbon dioxide separation and capture: A review*. 2008. **20**(1): p. 14-27.
- [9]. Baker, R.W.J.I. and e.c. research, *Future directions of membrane gas separation technology*. 2002. **41**(6): p. 1393-1411.
- [10]. Aaron, D., C.J.S.s. Tsouris, and technology, *Separation of CO₂ from flue gas: a review*. 2005. **40**(1-3): p. 321-348.
- [11]. Yu, C.-H., et al., *A review of CO₂ capture by absorption and adsorption*. 2012. **12**(5): p. 745-769.
- [12]. Bernardo, P., et al., *Membrane gas separation: a review/state of the art*. 2009. **48**(10): p. 4638-4663.
- [13]. Paul, D.R., *Polymeric gas separation membranes*. 2018: CRC press.
- [14]. Matteucci, S., et al., *Transport of gases and vapors in glassy and rubbery polymers*. 2006: p. 1-47.
- [15]. Chung, T.-S., et al., *Mixed matrix membranes (MMMs) comprising organic polymers with dispersed inorganic fillers for gas separation*. 2007. **32**(4): p. 483-507.
- [16]. McKeown, N.B.J.I.S.R.N., *Polymers of intrinsic microporosity*. 2012. **2012**.
- [17]. Freeman, B.D.J.M., *Basis of permeability/selectivity tradeoff relations in polymeric gas separation membranes*. 1999. **32**(2): p. 375-380.

- [18]. Robeson, L.M.J.J.o.m.s., *Correlation of separation factor versus permeability for polymeric membranes*. 1991. **62**(2): p. 165-185.
- [19]. Aoki, T.J.P.i.p.s., *Macromolecular design of permselective membranes*. 1999. **24**(7): p. 951-993.
- [20]. Javaid, A.J.C.E.J., *Membranes for solubility-based gas separation applications*. 2005. **112**(1-3): p. 219-226.
- [21]. Budd, P.M. and N.B.J.P.C. McKeown, *Highly permeable polymers for gas separation membranes*. 2010. **1**(1): p. 63-68.
- [22]. Tang, M.-W., W.M. King, and C.G. Wensley, *Air dried cellulose acetate membranes*. 1989, Google Patents.
- [23]. Deng, L., T.-J. Kim, and M.-B.J.J.o.M.S. Hägg, *Facilitated transport of CO₂ in novel PVAm/PVA blend membrane*. 2009. **340**(1-2): p. 154-163.
- [24]. Barlow, J., D.J.P.E. Paul, and Science, *Polymer blends and alloys—a review of selected considerations*. 1981. **21**(15): p. 985-996.
- [25]. Goh, P., et al., *Recent advances of inorganic fillers in mixed matrix membrane for gas separation*. 2011. **81**(3): p. 243-264.
- [26]. Hassan, A., M.U. Wahit, and C.Y.J.P.t. Chee, *Mechanical and morphological properties of PP/NR/LLDPE ternary blend—effect of HVA-2*. 2003. **22**(3): p. 281-290.
- [27]. Panapitiya, N., et al., *Compatibilized immiscible polymer blends for gas separations*. 2016. **9**(8): p. 643.
- [28]. Galizia, M., et al., *50th anniversary perspective: polymers and mixed matrix membranes for gas and vapor separation: a review and prospective opportunities*. 2017. **50**(20): p. 7809-7843.
- [29]. Vu, D.Q., W.J. Koros, and S.J.J.J.o.m.s. Miller, *Mixed matrix membranes using carbon molecular sieves: I. Preparation and experimental results*. 2003. **211**(2): p. 311-334.
- [30]. Zornoza, B., et al., *Metal organic framework based mixed matrix membranes: An increasingly important field of research with a large application potential*. 2013. **166**: p. 67-78.
- [31]. Wang, J., et al., *Graphitic carbon nitride nanosheets embedded in poly (vinyl alcohol) nanocomposite membranes for ethanol dehydration via pervaporation*. 2017. **188**: p. 24-37.

- [32]. Tian, Z., et al., *Enhanced gas separation performance of mixed matrix membranes from graphitic carbon nitride nanosheets and polymers of intrinsic microporosity*. 2016. **514**: p. 15-24.
- [33]. Mischnick, P., D.J.A.i.c.c. Momcilovic, and biochemistry, *Chemical structure analysis of starch and cellulose derivatives*. 2010. **64**: p. 117-210.
- [34]. Abedini, R., S.M. Mousavi, and R.J.D. Aminzadeh, *A novel cellulose acetate (CA) membrane using TiO₂ nanoparticles: preparation, characterization and permeation study*. 2011. **277**(1-3): p. 40-45.
- [35]. Sanaeepur, H., et al., *Cellulose acetate/nano-porous zeolite mixed matrix membrane for CO₂ separation*. 2015. **5**(3): p. 291-304.
- [36]. Hussain, A., et al., *Carbon capture from natural gas using multi-walled CNTs based mixed matrix membranes*. 2019. **40**(7): p. 843-854.
- [37]. Farrukh, S., et al., *Blending of TiO₂ nanoparticles with cellulose acetate polymer: to study the effect on morphology and gas permeation of blended membranes*. 2014. **9**(4): p. 543-551.
- [38]. Moghadassi, A., et al., *Fabrication and modification of cellulose acetate based mixed matrix membrane: Gas separation and physical properties*. 2014. **20**(3): p. 1050-1060.
- [39]. Ahmad, R., et al., *Cutting edge protein and carbohydrate-based materials for anticancer drug delivery*. 2018. **14**(1): p. 20-43.
- [40]. Bae, T.H., et al., *A high-performance gas-separation membrane containing submicrometer-sized metal-organic framework crystals*. 2010. **122**(51): p. 10059-10062.
- [41]. Ha, H., et al., *Gas permeation and selectivity of poly (dimethylsiloxane)/graphene oxide composite elastomer membranes*. 2016. **518**: p. 131-140.
- [42]. Gillan, E.G.J.C.o.m., *Synthesis of nitrogen-rich carbon nitride networks from an energetic molecular azide precursor*. 2000. **12**(12): p. 3906-3912.
- [43]. ZHANG, J.-S., B. WANG, and X.-C.J.A.P.-C.S. WANG, *Chemical synthesis and applications of graphitic carbon nitride*. 2013. **29**(9): p. 1865-1876.
- [44]. Cheng, L., et al., *g-C₃N₄ nanosheets with tunable affinity and sieving effect endowing polymeric membranes with enhanced CO₂ capture property*. 2020. **250**: p. 117200.

- [45]. Soto-Herranz, M., et al., *Effects of protonation, hydroxylamination, and hydrazination of g-C₃N₄ on the performance of matrimid®/g-C₃N₄ membranes*. 2018. **8**(12): p. 1010.
- [46]. Jomekian, A., et al., *Highly CO₂ selective chitosan/g-C₃N₄/ZIF-8 membrane on polyethersulfone microporous substrate*. 2020. **236**: p. 116307.
- [47]. Zhou, Y., et al., *Graphene oxide-modified g-C₃N₄ nanosheet membranes for efficient hydrogen purification*. 2021. **420**: p. 129574.
- [48]. Goldstein, J.I., et al., *Scanning electron microscopy and X-ray microanalysis*. 2017: Springer.
- [49]. Zhang, Y., et al., *Recent advances in gold nanostructures based biosensing and bioimaging*. 2018. **370**: p. 1-21.
- [50]. Noguchi, T.J.B.e.B.A.-B., *Fourier transform infrared difference and time-resolved infrared detection of the electron and proton transfer dynamics in photosynthetic water oxidation*. 2015. **1847**(1): p. 35-45.
- [51]. Ojeda, J.J., M.J.M.S.B.M. Dittrich, and Protocols, *Fourier transform infrared spectroscopy for molecular analysis of microbial cells*. 2012: p. 187-211.
- [52]. Hitkari, G., et al., *Nanoparticles: an emerging weapon for mitigation/removal of various environmental pollutants for environmental safety*. 2019: p. 359-395.
- [53]. Karim, S.S., et al., *Effects of coagulation residence time on the morphology and properties of poly (vinyl) alcohol (PVA) asymmetric membrane via NIPS method for O₂/N₂ separation*. 2020. **28**: p. 2810-2822.
- [54]. Wang, S., et al., *An image-driven finite element modeling method for evaluating the stress and strain distribution in carbon nanotubes/epoxy composites*. 2019. **6**(12): p. 125611.
- [55]. Azam, S.U., et al., *Enhancement in the selectivity of O₂/N₂ via ZIF-8/CA mixed-matrix membranes and the development of a thermodynamic model to predict the permeability of gases*. 2020. **27**: p. 24413-24429.
- [56]. Niu, P., et al., *Graphene-like carbon nitride nanosheets for improved photocatalytic activities*. 2012. **22**(22): p. 4763-4770.
- [57]. Butler, S.Z., et al., *Progress, challenges, and opportunities in two-dimensional materials beyond graphene*. 2013. **7**(4): p. 2898-2926.
- [58]. Zhao, X., et al., *Enhanced mechanical properties of graphene-based poly (vinyl alcohol) composites*. 2010. **43**(5): p. 2357-2363.

- [59]. Zhang, L., et al., *High strength graphene oxide/polyvinyl alcohol composite hydrogels*. 2011. **21**(28): p. 10399-10406.
- [60]. Kim, G.M., et al., *Relationship between morphology and micromechanical toughening mechanisms in modified polypropylenes*. 1996. **60**(9): p. 1391-1403.
- [61]. Li, J., et al., *A novel strategy for making poly (vinyl alcohol)/reduced graphite oxide nanocomposites by solvothermal reduction*. 2014. **54**: p. 520-525.
- [62]. Wang, X., et al., *A metal-free polymeric photocatalyst for hydrogen production from water under visible light*. 2009. **8**(1): p. 76-80.
- [63]. Cao, K., et al., *Highly water-selective hybrid membrane by incorporating g-C₃N₄ nanosheets into polymer matrix*. 2015. **490**: p. 72-83.
- [64]. Vinodhini, P.A., P.J.T. Sudha, and c. sustainability, *Removal of heavy metal chromium from tannery effluent using ultrafiltration membrane*. 2017. **2**(1): p. 1-15.
- [65]. Althumayri, K., et al., *The influence of few-layer graphene on the gas permeability of the high-free-volume polymer PIM-1*. 2016. **374**(2060): p. 20150031.